circulating cells expressing CEA mRNA. Clin Exp Metastasis 18:291–294
2. Hisatomi Y, Sugawara E, Nakano H, et al. (1999) Usefulness of various mRNAs detected as hematogeneously metastatic markers. SRL HOKAN (SRL Treasury) 23:109–112
3. Nordgard O, Aloysius TA, Todnem K, et al. (2003) Detection of lymph node micro metastases in colorectal cancer. Scand J Gastroenterol 2:125–132
4. Mellado B, Colomer D, Castel T, et al. (1996) Detection of circulating neoplastic cells by reverse-transcriptase polymerase chain reaction in malignant melanoma: association with clinical stage and prognosis. J Clin Oncol 14:2091–2097
5. Peilin H, Jingmei W, Ying G, et al. (2003) Molecular detection of disseminated tumor cells in the peripheral blood in patients with gastrointestinal cancer. J Cancer Res Clin Oncol 129:192–198
6. Maria GP, Filippo N, Daniela B, Piva MG, Navaglia F, Basso D (2000) CEA mRNA identification in peripheral blood is feasible for colorectal, but not for gastric or pancreatic cancer staging. Oncology 59:323–328
7. Masson D, Denis MG, Lustenberger P (2000) Limitation of CD44v6 amplification for the detection of tumor cells in the blood of colorectal cancer patients. Br J Cancer 82:1283–1289
8. Stathopoulou A, Mavroudis D, Perraki M, et al. (2003) Molecular detection of cancer cells in the peripheral blood of patients with breast cancer: comparison of CK-19, CEA and Maspin as detection markers. Anticancer Res 23:1883–1890
9. Takeda S, Ichii S, Nakamura Y (1993) Detection of K-ras mutation in sputum by mutant-allele-specific amplification (MASA). Hum Mutat 2:112–117
10. Nomoto S, Nakao A, Kasai Y, et al. (1996) Detection of ras gene mutation in preoperative peripheral blood with pancreatic adenocarcinoma. Jpn J Cancer Res 87:793–797
11. Gunn J, McCall JL, Yunk K, et al. (1996) Detection of micro metastases in colorectal cancer patients by CK19 and CK20 reverse transcription polymerase chain reaction. Lab Invest 75:611–616
12. Marc GD, Cecile L, Joel L, Paul-Antoine L, Denis MG, Lipart C, Leborgue J (1997) Detection of disseminated tumor cells in peripheral blood of colorectal cancer patients. Int J Cancer 74:540–544
13. Maria GP, Filippo N, Daniela B, et al. (2000) CEA mRNA identification in peripheral blood is feasible for colorectal, but not for gastric or pancreatic cancer staging. Oncology 59:323–328
14. Miura M, Ichikawa Y, Tanaka K, et al. (2003) Real-time PCR (TaqMan PCR) quantification of carcinoembryonic antigen (CEA) mRNA in the peripheral blood of colorectal cancer patients. Anticancer Res 23:1271–1276
15. Tabuchi Y, Nakae S, Imanishi K, et al. (1984) A clinicopathological study on the hematogenous recurrence of colorectal cancer – with special reference to the prediction and prevention of the recurrence. J Jpn Surg Soc 85:1359–1369
16. Maruyama K, Ochiai A, Nakamura S, et al. (1998) Dysfunction of E-cadherin system in invasion and metastasis of colorectal cancer. J Jpn Surg Soc 99:402–408
17. Schipper JH, Frixen UH, Behrens J, et al. (1991) E-cadherin expression in squamous cell carcinomas of head and neck: inverse correlation with tumor differentiation and lymph node metastasis. Cancer Res 52:6328–6337
18. Katsumata K, Yamamoto K, Murano A, et al. (1999) Correlation between adhesion molecules (laminin, sialyl Le^a, intercellular adhesion molecule-1), agglutination activity of platelet (11-dehydro-thromboxane B^2), and metastasis. J Jpn Soc Colo-Proctol 52:200–2002

Journal of Molecular Diagnostics, Vol. 8, No. 4, September 2006

DOI: 10.2353/jmoldx.2006.060030

Rapid and Simple Detection of Hot Spot Point Mutations of Epidermal Growth Factor Receptor, BRAF, and NRAS in Cancers Using the Loop-Hybrid Mobility Shift Assay

Shoichi Matsukuma,* Mitsuyo Yoshihara,* Fumio Kasai,* Akinori Kato,* Akira Yoshida,† Makoto Akaike,† Osamu Kobayashi,† Haruhiko Nakayama,† Yuji Sakuma,* Tsutomu Yoshida,‡ Yoichi Kameda,§ Eiju Tsuchiya,* and Yohei Miyagi*‡

From the Division of Molecular Pathology and Genetics, Kanagawa Cancer Center Research Institute, and the Division of Surgery,† the Laboratory for Molecular Diagnostics,‡ and the Division of Pathology,§ Kanagawa Cancer Center Hospital, Yokohama, Japan*

A simple and rapid method to detect the epidermal growth factor receptor hot spot mutation L858R in lung adenocarcinoma was developed based on principles similar to the universal heteroduplex generator technology. A single-stranded oligonucleotide with an internal deletion was used to generate heteroduplexes (loop-hybrids) bearing a loop in the complementary strand derived from the polymerase chain reaction product of the normal or mutant allele. By placing deletion in the oligonucleotide adjacent to the mutational site, difference in electrophoretic mobility between loop-hybrids with normal and mutated DNA was distinguishable in a native polyacrylamide gel. The method was also modified to detect in-frame deletion mutations of epidermal growth factor receptor in lung adenocarcinomas. In addition, the method was adapted to detect hot spot mutations in the B-type Raf kinase (BRAF) at V600 and in a Ras-oncogene (NRAS) at Q61, the mutations commonly found in thyroid carcinomas. Our mutation detection system, designated the loop-hybrid mobility shift assay was sensitive enough to detect mutant DNA comprising 7.5% of the total DNA. As a simple and straightforward mutation detection technique, loop-hybrid mobility shift assay may be useful for the molecular diagnosis of certain types of clinical cancers. Other applications are also discussed. *(J Mol Diagn 2006, 8:504–512; DOI: 10.2353/jmoldx.2006.060030)*

Rapid and accurate detection of mutations in various cancer-related genes has become increasingly important to provide molecular diagnostic information about clinical cancers. For example, information of the mutated states of particular genes is crucial for successful chemotherapy with certain gene-targeting drugs. Namely, gleevec (imatinib) has been shown to be effective for gastrointestinal stromal tumor with specific mutations in KIT[1,2] and PDGFRA,[3] as well as for chronic myelogenous leukemia carrying the chimeric gene BCR/ABL1.[4] Recently, a subset of lung adenocarcinomas with specific mutations in epidermal growth factor receptor (EGFR) has been reported to respond remarkably well to Iressa (gefitinib).[5–9]

To detect mutations in these and other oncogenes, there are several long-standing methods available such as direct sequencing of polymerase chain reaction (PCR)-amplified DNA, single-strand conformation polymorphism (SSCP),[10] SSCP/duplex analyses,[11] mutant allele-specific amplification,[12] and denaturing high performance liquid chromatography.[13,14] These techniques have been successfully applied for the detection of mutational changes in various cancer genes. Each method has its own advantages as well as disadvantages or difficulties in practical situations. Direct sequencing of heterozygous point mutations and deletions may produce results requiring sophisticated data analysis for heterozygous mutations, especially in the presence of contaminating normal tissue DNA. SSCP, widely used for its simplicity, requires strict temperature control during a long electrophoretic time and radiolabeling in standard detection. SSCP/duplex and denaturing high performance liquid chromatography analyses necessitate sophisticated separation equipment such as capillary electrophoresis or high performance liquid chromatography with temperature control. Mutant allele-specific amplification requires several primers with mutational sites at the 3′ ends to discriminate the mutational base changes by the lack of polymerase extension beyond the mis-

Supported by the Kanagawa Cancer Research Fund.

Accepted for publication May 22, 2006.

Address reprint requests to Dr. Shoichi Matsukuma, Division of Molecular Pathology and Genetics, Kanagawa Cancer Center Research Institute, Nakao 1-1-2, Asahi-ku, Yokohama 241-0815, Japan. E-mail: matsukum@gancen.asahi.yokohama.jp.

matched end, and occasional read-through can cause ambiguous results.

Heteroduplex analysis using universal heteroduplex generator (UHG) technology[15,16] is based on the retarded mobility in native polyacrylamide gel electrophoresis (PAGE) of a heteroduplex between the test PCR fragment and the PCR fragment termed the heteroduplex generator. Heteroduplex generators contain small deletions in the vicinities of mutational sites and generate four kinds of heteroduplexes with mutant and normal strands by hybridization, which are differentiated by the mobility changes. The method was applied to detect point mutations in sickle-cell diseases and phenylketonuria. Recently, UHG technology was adapted for detection of point mutations in NRAS at codons 12, 13, and 61.[17,18] In UHG technology, band patterns of four different retarded bands in PAGE are analyzed to determine mutational states. We simplified UHG technology by using single-stranded oligonucleotides with internal deletions as the generators of the loop-bearing heteroduplexes. This modification yields two bands for heterozygosity and one band for homozygosity, enabling more straightforward data analysis. Our method, designated the loop-hybrid mobility shift assay (LH-MSA), was developed to detect the point mutation L858R of EGFR exon 21 in lung adenocarcinoma that is associated with responsiveness to gene-targeted kinase inhibitors such as gefitinib. Adaptations of LH-MSA to detect in-frame deletions of EGFR exon 19 in lung adenocarcinoma and hot spot point mutations of BRAF and NRAS in thyroid carcinoma are also described.

Materials and Methods

DNA Preparations and Plasmid Clones

DNA from fresh tumor tissues (16 cases of lung adenocarcinoma, 25 cases of papillary thyroid carcinoma, and 19 cases of follicular thyroid carcinoma) was prepared according to standard protocols after obtaining informed consent. Formalin-fixed, paraffin-embedded (FFPE) tissue sections of lung adenocarcinoma and papillary thyroid carcinoma were also used for preparing DNA as follows. Thin-sectioned tissues (15 to 20 μm thick) were deparaffinized with xylene followed by ethanol series and air-dried. Tumor tissues, identified in the hematoxylin and eosin-stained serial sections (2 μm), were applied with a pinpoint solution (Pinpoint slide DNA isolation system; Zymo Research, Orange, CA), air-dried, and cut out together with the overlaid dried film of the pinpoint solution. The excised tissues (3-mm square) were digested in proteinase K buffer solution at 55°C for 4 hours, heat inactivated at 95°C for 15 minutes, and used as PCR template directly, or after purification with a spin column.

PCR-amplified DNA fragments were ligated to the TOPO-TA ligation vector pCR4TOPO (Invitrogen, Carlsbad, CA), electroporated into *Escherichia coli*, and cloned. Cloned bacterial cells were suspended in lysis solution (CloneChecker; Invitrogen), heat-lysed at 98°C for 30 seconds, and used as the cloned plasmid DNA solutions. DNA of the cloned plasmids was amplified with Phi29 polymerase (GE Health Care Bio-Science, Piscataway, NJ) and used for sequencing the inserts of tumor DNA fragments (CEQ8000 sequence analysis system; Beckman Coulter, Fullerton, CA). Direct sequencing of the PCR products from EGFR exon 21 was performed as described by Lynch and colleagues.[6]

Loop-Hybrid Formation in the LH-MSA

The LH-MSA consisted of two parts: hybridization of PCR products to the loop-hybrid generator (LH-G) probes made from synthetic oligonucleotides (70 to 99 mers) to generate loop-hybrids (Figure 1A) and analysis of mobility shifts of the loop-hybrids after native PAGE as described below. Nucleotide sequences of PCR primers and LH-G probes used to detect point mutations (7R, 18R, 9F, and 10K) and deletions (19JWTF) are described in Table 1. Each LH-G probe was designed to overlap with one of the PCR primer pairs at the 5′ end, and a stretch of up to 18 nucleotides was deleted in the region adjacent to the mutational hot spot for detection of point mutations. To detect deletion mutations in EGFR exon 19, the LH-G probe (19JWTF) was an oligonucleotide with no internal deletion that extended 26 nucleotides beyond the region of deletion mutations so that a loop forms only when it hybridizes with PCR products containing a deletion in EGFR exon 19 (Figure 3A). LH-G probes were purified with high performance liquid chromatography. PCR was performed with Accuprime *Taq* polymerase containing primer-template hybridization-enhancing reagent (Invitrogen). Generation of loop-hybrids was conducted at the end of the PCR amplification cycles by adding a specific LH-G probe into the PCR reaction solution at a final concentration of 500 nmol/L, ie, in large excess to the initial concentration of primer pairs (200 nmol/L). The mixture was then subjected to the loop-hybrid formation (LH-F) steps, consisting of 1) denaturation at 94°C for 2 minutes, 2) hybridization of the LH-G probe to the complementary strand at 55°C for 15 seconds, and 3) extension of the 3′ end of the LH-G probe in loop-hybrids by *Taq* polymerase at 68°C for 4 minutes. After the LH-F steps, reaction products were analyzed by PAGE to detect migration shift of the loop-hybrid bands by the mutations.

Detection of Loop-Hybrid DNA with PAGE

PCR products subjected to LH-F steps in the presence of LH-G probes were separated by electrophoresis in a native 10% polyacrylamide gel (6 cm × 6 cm preformed compact gels; ATTO Inc., Tokyo, Japan) in Tris-glycine buffer (37.5 mmol/L Tris, 288 mmol/L glycine) at 20 mA for 30 minutes at room temperature. Using a native 8% polyacrylamide gel in TBE buffer (89 mmol/L Tris, 89 mmol/L boric acid, 2 mmol/L ethylenediaminetetraacetic acid), electrophoresis of the loop-hybrid DNA performed at 10 mA for 1 hour at room temperature yielded equivalent results. After electrophoresis, gels were stained for 10 minutes with SYBER Green I (Cambrex Bio Science, Rockland, ME) diluted to 1/10,000 in distilled water and

Table 1. PCR Primers and LH-G Probes Used for Detection of Mutations in EGFR, BRAF, and NRAS

Gene	Mutation	Amplicon	PCR primer†	LH-G probe‡ (probe name)
EGFR	In-frame deletion in exon 19	212bp	(F) GGACTCTGGATCCCAGAAGGTG	GGACTCTGGA TCCCAGAAGG TGAGAAAGTT
				AAAATTCCCG TCGCTATCAA GGAATTAAGA
			(R) CATTTAGGATGTGGAGATGAGC	GAAGCAACAT CTCCGAAAGC CAACAAGGAA
				ATCCTCGAT (19JWTF)
EGFR	Point mutation in exon 21 at L858	161bp	(F) GGCATGAACTACTTGGAGGAC	CTTACTTTGC CTCCTTCTGC ATGGTATTCT
				TTCTCTTCCG CACCCAGCAG *******AGC
			(R) CTTACTTTGCCTCCTTCTGCATG	CCAAAATCTG TGATCTTGAC ATGCTGCG
				(7R)
				CTTACTTTGC CTCCTTCTGC ATGGTATTCT
				TTCTCTTCC* ********** *******AGC
				CCAAAATCTG TGATCTTGAC ATGCTGCG
				(18R)
BRAF	Point mutation in exon 15 at V600	157bp	(F) ATTTCTTCATGAAGACCTCACAG	ATTTCTTCAT GAAGACCTCA CAGTAAAAAT
				AGGTGATTTT GGTCTAGCTA CAGT******
			(R) GGCCAAAAATTTAATCAGTGGA	***ATGGAGT GGGTCCCATC AGTTTG
				(9F)
NRAS	Point mutation at 061	149bp	(F) GTGAAACCTGTTTGTTGGAC	GTGAAACCTG TTTGTTGGAC ATACTGGATA
				CAGCTGGACA ********** AGTGCCATGA
			(R) CCTGTAGAGGTTAATATCCG	GAGACCAATA CATGAGGACA GG (10K)

†(F), forward primers; (R), reverse primers.
‡*, deleted nucleotides; underlined nucleotides indicate the hot spots of mutations to be detected.

placed in deionized water to remove excess dye. After the staining, DNA was detected with a laser-scanning imager (STORM860; GE Health Care Bio-Science) using 450-nm excitation and a 520-nm long path filter. A 100-bp ladder (Promega, Madison, WI) was used to distinguish the bands of loop-hybrid DNA showing retarded migration from the homoduplex bands showing size-dependent migration.

Estimation of Mutant Copy Numbers with LH-MSA

Plasmid clones of PCR products from the L858R mutant and normal alleles of EGFR exon 21 were mixed together at mutant to normal ratios ranging from 1 to 0.05. After PCR of these mixed samples with Accuprime *Taq* High Fidelity (Invitrogen), an aliquot was examined directly with LH-MSA using the 18R LH-G probe to determine the sensitivity of mutation detection and the remaining portion was used for TOPO-TA ligation and cloning as described above. Forty-eight to ninety-six bacterial clones were genotyped with LH-MSA using the 18R LH-G probe to estimate copy numbers of the mutant allele in PCR products from the mixed samples. No mutant was found in the 48 clones of the normal control. Dideoxy sequencing of the mixed plasmid DNA was performed as described above.

Results

Detection of the EGFR Hot Spot Mutation L858R in Lung Adenocarcinoma Using LH-MSA

For simple and easy detection of the point mutation at L858 in EGFR exon 21, a method similar to the universal heteroduplex generator technology[15–18] was developed. As illustrated in Figure 1A, the heteroduplex with a loop (hereafter referred to as loop-hybrid) can be generated by hybridization of the PCR product from EGFR exon 21 with a synthetic oligonucleotide (LH-G probe) having a stretch of nucleotides deleted adjacent to the mutation hotspot at L858. A series of LH-G probes expected to generate loops of various nucleotide lengths (Figure 1B) was examined. Migration of the loop-hybrids in PAGE was markedly retarded compared to the size-dependent migration of the homoduplex, and the degree of retarded mobility depended on the size of loop in the loop-hybrid (Figure 1, B and C). The loop-hybrid band of the mutant allele was markedly shifted from that of the normal allele when the same LH-G probe was used (Figure 1B). The shift was particularly pronounced for the LH-G probes 4R, 7R, 14R, and 18R. Faint secondary bands were visible beside the major LH band when the LH-G probes 3R, 6R, and 8R were used. DNA from the retarded bands excised from the gel was amplified with PCR and cloned into plasmids. When these clones were sequenced, both the original PCR fragment and the derivative of the LH-G probe used to generate the loop-hybrid were identified (data not shown), confirming our model (Figure 1A). When the faint secondary band produced by LH-G probe 8R was similarly analyzed, a mutation (one base deletion five bases upstream of the internally deleted site) was detected in the sequence corresponding to the 8R LH-G probe, whereas the expected sequence of 8R was found in the main loop-hybrid band. Therefore, the faint secondary band seemed to be generated by a contaminating mutant form of the 8R LH-G probe. Purification of LH-G probes with PAGE may be necessary to reduce such inadvertent contaminants. The LH-G probes 7R and 18R showed single, discrete loop-hybrid bands, well distinguishing the mutant from the normal allele and distinctly separated from the homoduplex band. Therefore, these LH-G probes were adopted in the following LH-MSA analysis to detect the L858R mutation in EGFR exon 21. Heterozygous mutations are detected as the double bands of the normal and the shifted mutant loop-hybrid bands.

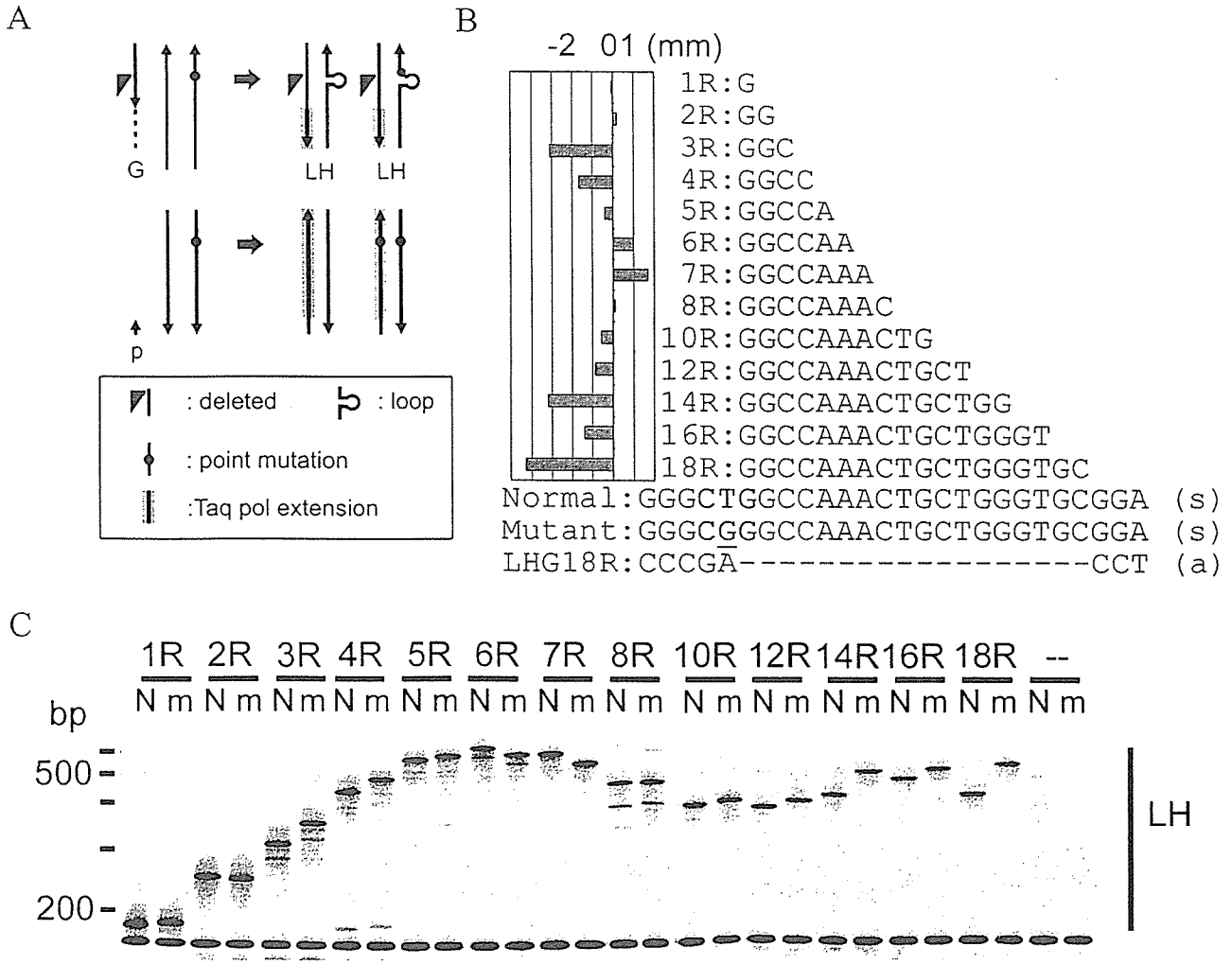

Figure 1. Detection of the hot spot point mutation L858R (CTG>CGG) of EGFR exon 21 by LH-MSA using various LH-G probes. **A:** Schematic representation of loop-hybrids (LH) generated by an LH-G probe (G) in the PCR product heterozygous for a point mutation. Homoduplexes of the normal and mutant alleles are produced by polymerase extension of the hybridized PCR primer (p). The broken line indicates the 3′ region of the UH-G probe to be extended by *Taq* polymerase after hybridization. **Gray arrows** indicate the hybridizing reaction. **B:** Mobility shifts of the loop-hybrid bands caused by the mutant allele are shown as the difference (mm) in mobility in the gel between the loop-hybrid band of the mutant allele and that of the normal allele for each LH-G probe, together with the sequence of the loop generated by the LH-G in the sense strand of the normal allele. Partial sequences of the normal and mutant alleles in the sense (s) strand are shown, with the codon L858 in bold. Also shown is the partial reverse anti-sense sequence (a) of the LH-G probe 18R with deleted nucleotides (−). **C:** Paired PCR products from the template DNA of the plasmid clones of the normal (N) and the mutated (m) alleles were examined with a series of LH-G probes as denoted for each lane and analyzed with PAGE. Deletions in these LH-G probes generated the loops of 1 to 18 nucleotide lengths in the loop-hybrids. Control PCR products (−) hybridized with no LH-G probe are also shown.

DNA prepared from fresh lung adenocarcinoma tumor tissues was screened for the L858R mutation using LH-MSA (Figure 2A). The expected double bands for the putatively heterozygous mutation were clearly shown for 3 of 16 examined cases. The L858R mutation in these three cases was confirmed by direct sequencing. For comparison DNA from FFPE tissues of 50 cases in pathological archives of operated lung adenocarcinoma were analyzed by LH-MSA and by direct sequencing. PCR products from those cases in which mutations were detected by LH-MSA were cloned in plasmids and screened with LH-MSA, and mutant clones were sequenced. As summarized in Table 2, 26% of the cases (13 of 50) exhibited the L858R mutation. Nine of these were consistent with the direct sequencing results, but the remaining four were not confirmed because of insufficient quality of the direct sequence data. One mutation (2%) other than L858R was detected by LH-MSA and determined to be A859T by sequence analysis of the mutant clone and by the direct sequencing. When FFPE tissue DNA from an additional 68 lung adenocarcinoma cases was examined by LH-MSA, the mutation L858R was again observed at a high frequency (27.9%, Table 2). Mutations other than L858R (L861R) were detected at a low frequency (2.9%, 2 of 68) by LH-MSA and sequence analysis of the mutant clones. One of the rare mutations (L861R) produced a mutant loop-hybrid band that shifted differently from that of L858R (Figure 2B). These rare mutations were close in proximity to L858 (Figure 2C). In the present analysis, the mutational state of EGFR exon 21 at L858 was diagnosed by LH-MSA with a high accuracy of 97.5%, taking into account mutations other than L858R (2.5%). Mutations other than

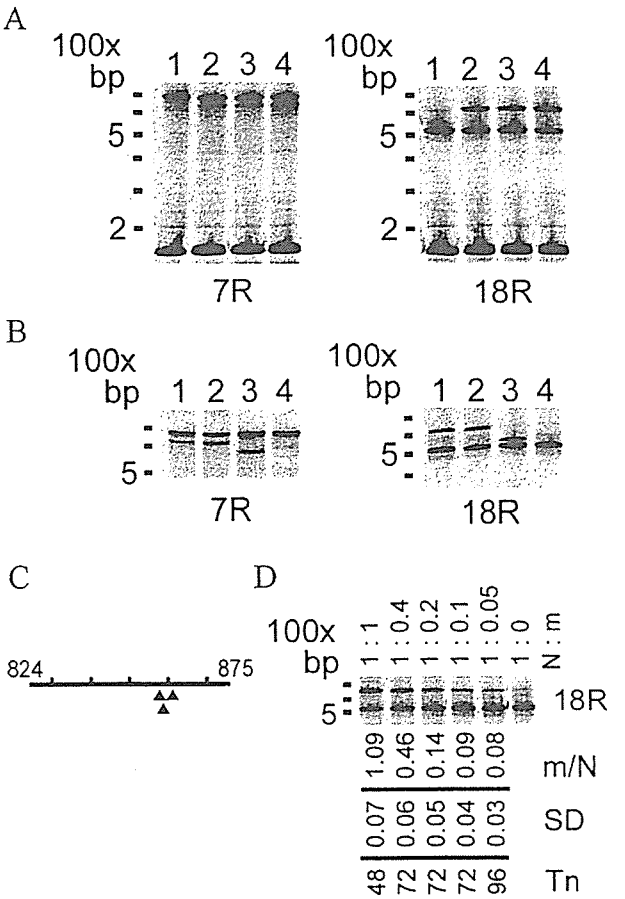

Figure 2. Detection of point mutations at or near the hot spot L858 of EGFR exon 21. **A:** The electropherogram after LH-MSA using LH-G probes 7R and 18R to detect the L858R mutation (CTG>CGG) of EGFR exon 21 in DNA from fresh lung adenocarcinoma tissues. **Lane 1**, the normal allele; **lanes 2** to **4**, putative heterozygous mutations. The homoduplex bands were 161 bp in length. **B:** LH-MSA with probes 7R and 18R to detect the following heterozygous mutations in EGFR exon 21 of L858R (CTG>CGG, **lane 1**), A859T (GCC>ACC, **lane 2**), and L861R (CTG>CGG, **lane 3**). **Lane 4** is the normal allele. **C:** Positions of point mutations in exon 21 detected by LH-MSA (L858R, A859T, L861R; closed triangles). **D:** Detection of the mutated allele (m) of EGFR L858R present at decreasing ratios to the normal allele (N) with LH-MSA using the LH-G probe 18R. The template DNA was constituted by mixing the diluted DNA of cloned plasmids of the mutated and normal alleles. Loop-hybrid bands are shown, together with the observed mutant to normal ratios (m/N) in the PCR products, the standard deviations (SDs), and the total numbers of clones examined (Tn).

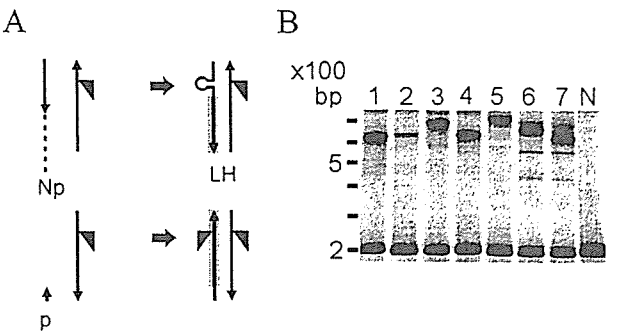

C

```
G1 ATCAAGGAA.........CCAACATCTCCGAAA(15)
G2 ATCAA.............AACATCTCCGAAA(17)
G3 ATCAAG............ACATCTCCGAAA (6)
G4 ATCAAGGAAT............CTCCGAAA (4)
G5 ATCAAGG..............TTCCGAAA (1)
G6 ATCAAGGAA..............CCGAAA (1)
G7 ATCAAGGAAT.............CGAAA (1)
N  ATCAAGGAATTAAGAGAAGCAACATCTCCGAAA
     I  K  E  L  R  E  A  T  S  P  K
```

Figure 3. Detection of deletion mutations in EGFR exon 19 with LH-MSA. **A:** Schematic representation of loop-hybrids (LH) generated by the normal LH-G probe (Np) hybridized to the anti-sense strands of the PCR products of deleted mutant alleles. Homoduplexes of the deleted mutants are reproduced in LH-MSA by extension of the PCR primer (p) hybridized to the sense strands of the PCR products. The symbols are the same as in Figure 1A. **B:** LH-MSA of PCR products from the plasmid clones of deletion mutant alleles G1 to G7 (**lanes 1** to **7**) and of the normal allele (N) treated with the normal LH-G probe 19JWTF. **C:** Partial nucleotide sequences of the deletion mutants (G1 to G7) and the normal allele (N) of EGFR exon 19, as well as the corresponding normal amino acid sequence. Deleted nucleotides are indicated by dots, and nucleotide displacements are underlined. Incidences of the single deleted mutations in 118 cases of lung adenocarcinoma are shown in parentheses.

L858R that were undetected by LH-MSA could occur, but their presence was not verified in this study.

LH-MSA may be used semiquantitatively, as shown in Figure 2D. The mutant allele in the mixed sample at the mutant to normal ratio 0.05 (0.08 by the observed ratio) was detected with LH-MSA but not detected by dideoxy sequencing (data not shown). Our results show that LH-MSA was able to detect a mutant allele comprising 7.5% of the total DNA, suggesting that tumor cells with a heterozygous mutation that comprise 15% of the total cell mixture might be detected by LH-MSA.

Detection of In-Frame Deletion Mutations in Lung Adenocarcinoma Using LH-MSA

In-frame deletion mutations in EGFR exon 19 involving 9 to 18 bases (including the overlapping region L747 to E749; Figure 3C) were detected frequently in lung adenocarcinoma.[5–9] For heterozygous deletion mutations, heteroduplexes between the normal and the deleted mutant alleles of the PCR product were detected in PAGE as

Table 2. Point Mutations in EGFR Exon 21 Detected by LH-MSA in FFPE Tissue DNA from Lung Adenocarcinomas

Genotype of EGFR exon 21	Experiment 1		Experiment 2	Total
	LH-MSA (%)	Direct sequence (%)	LH-MSA (%)	LH-MSA (%)
Normal	36 (72)	35 (70)	47 (69.1)	83 (70.3)
L858R	13 (26)	9 (18)	19 (27.9)	32 (27.1)
A859T	1 (2)	1 (2)		1 (0.8)
L861R			2 (2.9)	2 (1.7)
Undetermined		5 (10)		
Total	50	50	68	118

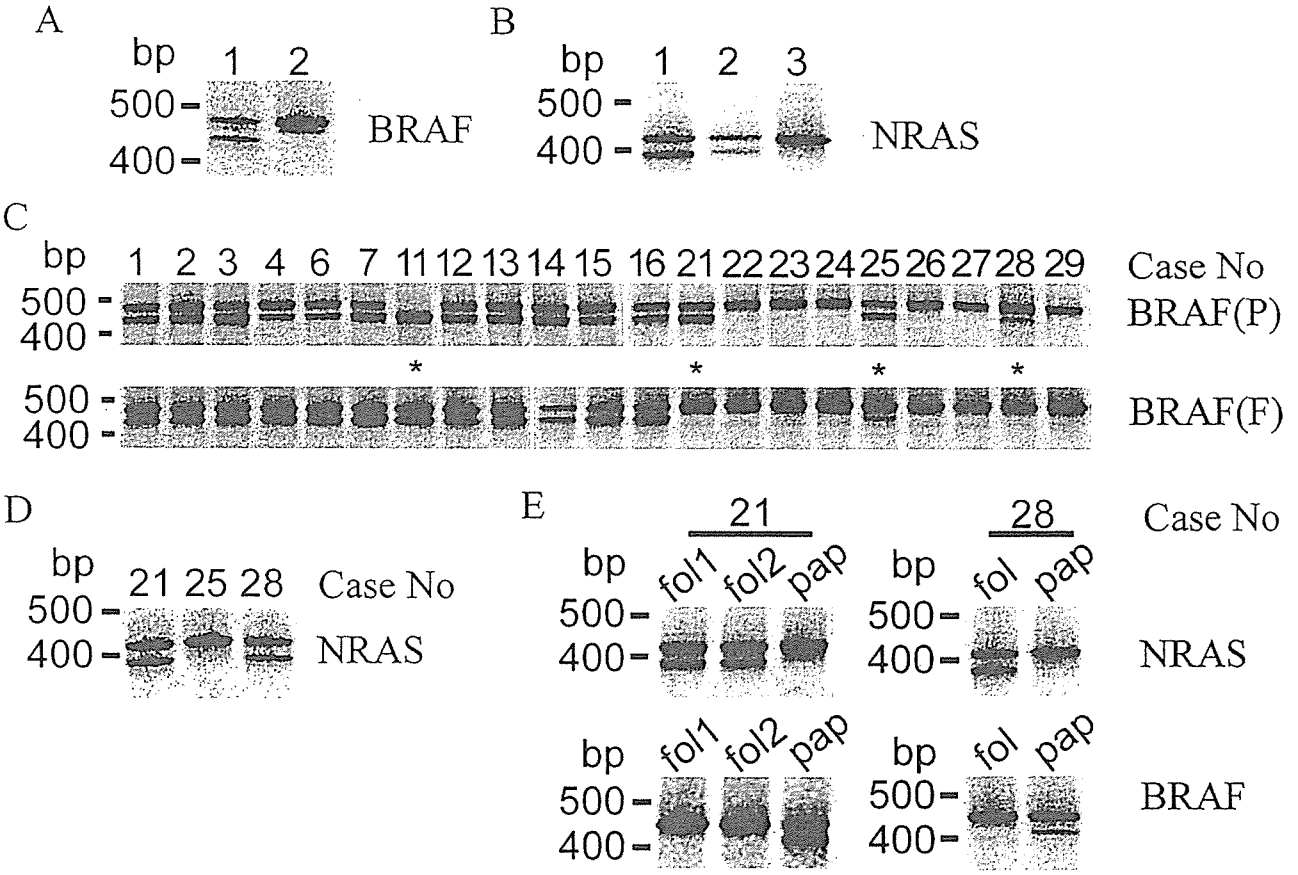

Figure 4. Comparison of the mutations in BRAF at V600 and NRAS at Q61 detected by LH-MSA in DNA derived from bulk fresh tumor tissues versus FFPE tumor tissues of thyroid carcinoma. **A:** Loop-hybrid bands after LH-MSA with the LH-G probe 9F for detection of the mutation V600E (GTG>GAG) in BRAF exon 15, using the DNA from fresh tumor papillary thyroid carcinoma tissue. **Lane 1**, the putative heterozygous BRAF mutation; **lane 2**, the normal allele. **B:** Loop-hybrid bands after LH-MSA with the LH-G probe 10K for detection of mutations in NRAS at Q61, using DNA from fresh tumor follicular thyroid carcinoma tissue. **Lanes 1** and **2**, the putative heterozygous NRAS mutations Q61R (CAA>CGA) and Q61K (CAA>AAA), respectively; and **lane 3**, the normal allele. **C:** Loop-hybrid bands for detection of the BRAF mutation V600E, using DNA from FFPE tumor tissues (P) and from bulk fresh tumor tissues (F) of 21 thyroid papillary carcinoma cases. **Asterisks** indicate discrepant results. **D:** Loop-hybrid bands after LH-MSA for detection of the NRAS mutation Q61R in bulk fresh tumor DNA of the discrepant cases with respect to the BRAF mutation. The heterozygous NRAS mutation was evident in cases 21 and 28. **E:** Loop-hybrid bands indicating the heterozygous NRAS mutation Q61R (top) and the heterozygous BRAF mutation V600E (bottom) in DNA derived from follicular-type (fol1, fol2, and fol) and papillary-type (pap) tumors of FFPE tissue sections in the discrepant cases 21 and 28.

a pair of retarded mobility bands easily distinguishable from the homoduplex band showing size-dependent migration (data not shown). LH-MSA was adapted to detect not only heterozygous but also mono-allelic deletion mutations (Figure 3A). Namely, a normal oligonucleotide, 19JWTF, was added as the LH-G probe to the PCR products from plasmid clones of several deleted mutant alleles and hybridized using LH-F steps. Analysis of these reaction products in PAGE revealed various retarded mobility bands of loop-hybrids at specific positions for each of the deleted mutant alleles (Figure 3B). No retarded mobility band was observed for the PCR product of the normal allele treated with this LH-G probe. Using this LH-MSA adapted for the detection of deletion mutations in EGFR exon 19, 49 deletion mutations (41.5%) were detected in DNA samples from FFPE tumor tissues of 118 lung adenocarcinoma cases and these deletions were confirmed by sequencing the cloned mutants. Although most of the cases (45 of 49, 92%) were uniquely associated with one of the deletion mutations shown in Figure 3C, composite mutations of two different in-frame deletions were also found after sequencing mutant clones. They were composed of G1 and G2 (two cases), G1 and G3 (one case), and G1 and G4 (one case) (Figure 3C). These observations implicated multiple mutations in these tumor cases.

Detection of BRAF and NRAS Hot Spot Mutations in Thyroid Carcinoma Using LH-MSA

The kinase-activating mutation V600E in BRAF was shown to occur at high frequencies in papillary thyroid carcinoma,[19–21] whereas the activating mutation at Q61 in NRAS is prevalent in follicular thyroid carcinoma.[22,23] LH-MSA was adapted for detection of these mutations. DNA samples prepared from fresh tumor tissues of papillary thyroid tumors were examined by LH-MSA for the V600E BRAF mutation. Distinct double bands (Figure 4A), presumably indicating the heterozygous point mutation, were observed in 64% (16 of 25) of cases, consistent with the previous direct sequencing results. Similarly, DNA samples prepared from fresh tumor tissues of follicular thyroid carcinoma were screened for the NRAS

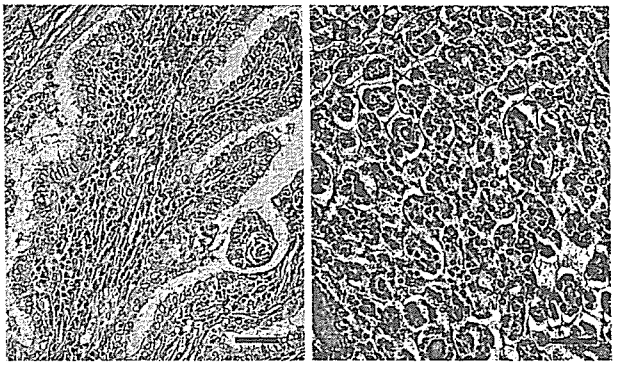

Figure 5. Different histopathological types of the thyroid tumor in case 28 in tissue sections stained with H&E. **A:** Tumor tissue of the papillary type. **B:** Tumor tissue of the follicular type. Scale bars = 50 μm.

Q61 mutations using LH-MSA. As shown in Figure 4B, distinct double bands were observed for the putative heterozygous mutations of Q61R and Q61K (26 and 5% of 19 cases, respectively), consistent with predetermined direct sequencing results.

DNA from fresh papillary thyroid carcinoma tumor tissues and from FFPE tumor tissues from the same cases was compared for consistency of the mutations detected by LH-MSA. Of 21 cases compared, 17 yielded the same results using both DNA samples, namely, the BRAF heterozygous V600E mutation in 11 cases and no such mutation in six cases. Discrepant results were observed in four cases (Figure 4C). In one case (no. 11), a single mutant loop-hybrid band was predominant in the FFPE tissue DNA, but heterozygous double bands were observed at equal densities in the fresh tumor DNA. Such differences may be attributed to the loss of heterozygosity in some portions of tumor tissues, including the sampled area of the paraffin section within the tumor heterozygous for the BRAF mutation. The faint shifted loop-hybrid band of the mutant allele in case 25 may suggest that the fresh tumor DNA was contaminated by DNA from normal cells, because equally dense double bands indicating the heterozygous BRAF mutation were detected in the FFPE tumor tissue DNA. In the other two cases (nos. 21 and 28), the normal BRAF in the bulk fresh tumor tissue DNA were discrepant with the apparently heterozygous BRAF mutation in the FFPE tissue DNA. Interestingly, NRAS mutation Q61R was detected in the bulk fresh tumor DNA in these two cases (Figure 4D) but not in the other 19 cases. Histopathological examinations of the tumors documented the presence of both of papillary and follicular tissue types as separate components in the same tumors in these two particular cases, but not in the others (Figure 5, A and B). Tumor DNA from these papillary and follicular tissue types were separately sampled from the FFPE tissue sections and examined for the mutations in BRAF and NRAS using LH-MSA. As shown in Figure 4E, double bands indicating the heterozygous BRAF mutation were detected in the papillary-type but not in the follicular-type tumor tissues. On the other hand, the double bands indicating the heterozygous NRAS mutation were detected in the follicular-type but not in the papillary-type tumor tissues. Because NRAS mutations tended to be associated with follicular thyroid carcinoma,[22,23] DNA prepared from fresh bulk tumors before histological diagnosis in the above two thyroid tumor cases seemed to be derived from the follicular-type tumors carrying the mutation in NRAS but not from the papillary-type tumors carrying the mutation in BRAF.

Discussion

LH-MSA is unique in that synthetic oligomers are used for the generation of heteroduplexes bearing small loops by hybridization to PCR products. Differential mobility of the loop-hybrids in native PAGE that reflects a slight change in the nucleotide adjacent to or within the loop was exploited to detect mutational changes present in the DNA. LH-MSA, along with the original UHG technology,[15–18] may provide a simple and useful system for detection of mutations in various cancers with fixed mutational hot spots. However, detection of widespread loss-of-function mutations in TP53, BRCA1, MLH1, and other cancer-related genes may elude straightforward application of LH-MSA in the present simple format. As shown in this study, LH-MSA is particularly useful for the molecular diagnosis of lung adenocarcinoma because it can easily detect in-frame deletion mutations in exon 19 and the hot spot point mutation L858R in exon 21 of EGFR that is associated with therapeutic responses to EGFR kinase inhibitors such as gefitinib.[5–9] The V600E point mutation in BRAF could be diagnostically important for thyroid carcinoma[19–21] and melanoma[24–26] if specific kinase inhibitor drugs for mutated BRAF become commonly available for therapeutic use.[27] LH-MSA was able to detect mutant alleles present at low proportions in the sampled DNA. This might be a valuable feature of LH-MSA for cases in which tumor cells are intermingled with varying amounts of normal cells in available diagnostic samples. Similar sensitivity in the detection of NRAS mutations at low proportions was also achieved using the standard UHG technology.[17,18]

Point mutations detectable with LH-MSA may not be limited to the genes presently described. Adaptations of LH-MSA to detect various point mutations of the Ras-oncogene KRAS at codons G12 to G13 in various cancers may be pursued. Genotyping of single nucleotide polymorphisms (SNPs) can also theoretically be achieved by LH-MSA at any loci, and adaptation of LH-MSA for various intragenic SNP loci is under investigation. LH-MSA could be incorporated in SNP analyses of risks such as hypersensitivity to certain therapeutic drugs[28,29] and susceptibility to cancers.[30]

LH-MSA is applicable to any unique genomic sequences amplified with PCR. LH-G probes to detect point mutations or to genotype SNPs can be designed using a simple hypothesis. Namely, a mismatched base at the site adjacent to the loop in the loop-hybrid will induce a shift in its mobility. Nucleotide lengths of the loop and the positions of the loop relative to the mutational site can be varied to attain optimal shifts of the loop-hybrid band in the presence of the mutation. A faint secondary band that

might confuse interpretation of the results may be virtually eliminated using PAGE-purified LH-G probes. Mutational changes occurring within the loops were detected by LH-MSA as shown for the mutations in EGFR, A859T, and L861R. These instances indicated that there might be some sensitive positions in the loop sequences such that a single nucleotide change therein may affect loop conformation and lead to a mobility shift of the loop-hybrid. In the present study, PAGE was executed at room temperature, and the influence of ambient temperature fluctuation on the retarded mobility of loop-hybrid DNA during electrophoresis appeared to be low. However, detection of mutations within the loops by LH-MSA seemed to be improved by lowering the temperature during electrophoresis (our preliminary observation).

To assess the reliability of LH-MSA for detecting mutations in the DNA of fixed tumor tissues, DNA prepared from fresh tumor tissues and from FFPE tissue sections was compared. Identical results were obtained for the deletion mutations in EGFR exon 19 of lung adenocarcinoma (data not shown). However, a few discrepant results were observed for the point mutation of BRAF in papillary thyroid carcinoma. In two cases, discrepancy was attributed to the presence of two distinct lines of differentiation in thyroid tumor development. The different histopathological types of tumors and their association with distinct mutations in the above two cases may indicate the existence of tumors that were initiated by a common cause but subsequently followed separate courses of tumor development by the mutations of different genes in RAS-RAF signaling pathway. Our detailed analysis not only resolved the discrepancies but also affirmed the tissue-type-specific associations of the BRAF mutation to papillary[19–21] and the NRAS mutation to follicular[22,23] thyroid carcinoma. The results for the unusual cases shown above clearly indicated that the DNA derived from FFPE tissues, although low in quality and quantity, could provide precise and important molecular data associated with histopathological diagnosis.

Single LH-bands for each of the mutant and normal alleles were sharp and well separated, and therefore seemed amenable to semiquantitative approaches such as copy number estimation. Simplicity of LH-MSA may allow instantaneous detection of mutations in comparison to other mutation detection systems such as SSCP and UHG, in which four bands derived from normal and mutant strands are usually exhibited. Compared with denaturing high performance liquid chromatography, LH-MSA showed a fourfold higher sensitivity in detection of the L858R mutation in EGFR when serially mixed samples were applied at a low concentration (our preliminary results). The simple LH-MSA detection system may enable rapid and low-cost screening of hot spot mutations in certain types of cancers and genotyping of SNPs in clinical risk assessment. LH-MSA and silver staining of the gel after PAGE may facilitate genetic examinations in minimal laboratory settings. Use of LH-MSA for genotyping analysis may not be limited to humans but might be extended to any organism. Current genome-wide searches for SNP loci associated with specific phenotypes and for mutations responsible for hereditary diseases in humans and domestic animals may be greatly facilitated by simple genotyping tools such as LH-MSA.

Acknowledgments

We thank Ms. Masako Teranishi and Ms. Kumiko Ohrui for their excellent technical assistance.

References

1. Hirota S, Isozaki K, Moriyama Y, Hashimoto K, Nishida T, Ishiguro S, Kawano K, Hanada M, Kurata A, Takeda M, Muhammad Tunio G, Matsuzawa Y, Kanakura Y, Shinomura Y, Kitamura Y: Gain-of-function mutations of c-kit in human gastrointestinal stromal tumors. Science 1998, 279:577–580
2. Joensuu H, Roberts P, Sarlomo-Rikala M, Andersson L, Tervahartiala P, Tuveson D, Silberman S, Capdeville R, Dimitrijevic S, Druker B, Demetri G: Effect of the tyrosine kinase inhibitor STI571 in a patient with a metastatic gastrointestinal stromal tumor. N Engl J Med 2001, 344:1052–1056
3. Heinrich M, Corless C, Duensing A, McGreevey L, Chen C, Joseph N, Singer S, Griffith D, Haley A, Town A, Demetri G, Fletcher C, Fletcher J: PDGFRA activating mutations in gastrointestinal stromal tumors. Science 2003, 299:708–710
4. Savage D, Antman K: Imatinib mesylate—a new oral targeted therapy. N Engl J Med 2002, 346:683–693
5. Arao T, Fukumoto H, Takeda M, Tamura T, Saijo N, Nishio K: Small in-frame deletion in the epidermal growth factor receptor as a target for ZD6474. Cancer Res 2004, 64:9101–9104
6. Lynch T, Bell D, Sordella R, Gurubhagavatula S, Okimoto R, Brannigan B, Harris P, Haserlat S, Supko J, Haluska F, Louis D, Christiani D, Settleman J, Haber D: Activating mutations in the epidermal growth factor receptor underlying responsiveness of non-small-cell lung cancer to gefitinib. N Engl J Med 2004, 350:2129–2139
7. Marchetti A, Martella C, Felicioni L, Barassi F, Salvatore S, Chella A, Camplese P, Iarussi T, Mucilli F, Mezzetti A, Cuccurullo F, Sacco R, Buttitta F: EGFR mutations in non-small-cell lung cancer: analysis of a large series of cases and development of a rapid and sensitive method for diagnostic screening with potential implications on pharmacologic treatment. J Clin Oncol 2005, 23:857–865
8. Paez J, Janne P, Lee J, Tracy S, Greulich H, Gabriel S, Herman P, Kaye F, Lindeman N, Boggon T, Naoki K, Sasaki H, Fujii Y, Eck M, Sellers W, Johnson B, Meyerson M: EGFR mutations in lung cancer: correlation with clinical response to gefitinib therapy. Science 2004, 304:1497–1500
9. Pao W, Miller V, Zakowski M, Doherty J, Politi K, Sarkaria I, Singh B, Heelan R, Rusch V, Fulton L, Mardis E, Kupfer D, Wilson R, Kris M, Varmus H: EGF receptor gene mutations are common in lung cancers from "never smokers" and are associated with sensitivity of tumors to gefitinib and erlotinib. Proc Natl Acad Sci USA 2004, 101:13306–13311
10. Orita M, Iwahana H, Kanazawa H, Hayashi K, Sekiya T: Detection of polymorphisms of human DNA by gel electrophoresis as single-strand conformation polymorphisms. Proc Natl Acad Sci USA 1989, 86:2766–2770
11. Kozlowski P, Krzyzosiak W: Combined SSCP/duplex analysis by capillary electrophoresis for more efficient mutation detection. Nucleic Acids Res 2001, 29:E71
12. Takeda S, Ichii S, Nakamura Y: Detection of K-ras mutation in sputum by mutant-allele-specific amplification (MASA). Hum Mutat 1993, 2:112–117
13. Underhill P, Jin L, Lin A, Mehdi S, Jenkins T, Vollrath D, Davis R, Cavalli-Sforza L, Oefner P: Detection of numerous Y chromosome biallelic polymorphisms by denaturing high-performance liquid chromatography. Genome Res 1997, 7:996–1005
14. Liu W, Smith D, Rechtzigel K, Thibodeau S, James C: Denaturing high performance liquid chromatography (DHPLC) used in the detection of germline and somatic mutations. Nucleic Acids Res 1998, 26:1396–1400
15. Wood N, Standen G, Hows J, Bradley B, Bidwell J: Diagnosis of

sickle-cell disease with a universal heteroduplex generator. Lancet 1993, 342:1519–1520
16. Wood N, Tyfield L, Bidwell J: Rapid classification of phenylketonuria genotypes by analysis of heteroduplexes generated by PCR-amplifiable synthetic DNA. Hum Mutat 1993, 2:131–137
17. Belli C, De Brasi C, Larripa I: Rapid detection of exon 1 NRAS gene mutations using universal heteroduplex generator technology. Hum Mutat 2003, 21:132–137
18. Belli C, Bowen D, De Brasi C, Larripa I: A single, multiplex analysis for all relevant activating NRAS gene mutations using heteroduplex generators. Br J Haematol 2004, 126:602–605
19. Cohen Y, Xing M, Mambo E, Guo Z, Wu G, Trink B, Beller U, Westra W, Ladenson P, Sidransky D: BRAF mutation in papillary thyroid carcinoma. J Natl Cancer Inst 2003, 95:625–627
20. Kimura E, Nikiforova M, Zhu Z, Knauf J, Nikiforov Y, Fagin J: High prevalence of BRAF mutations in thyroid cancer: genetic evidence for constitutive activation of the RET/PTC-RAS-BRAF signaling pathway in papillary thyroid carcinoma. Cancer Res 2003, 63:1454–1457
21. Xu X, Quiros R, Gattuso P, Ain K, Prinz R: High prevalence of BRAF gene mutation in papillary thyroid carcinomas and thyroid tumor cell lines. Cancer Res 2003, 63:4561–4567
22. Vasko V, Ferrand M, Di Cristofaro J, Carayon P, Henry J, de Micco C: Specific pattern of RAS oncogene mutations in follicular thyroid tumors. J Clin Endocrinol Metab 2003, 88:2745–2752
23. Nikiforova M, Lynch R, Biddinger P, Alexander E, Dorn IIG, Tallini G, Kroll T, Nikiforov Y: RAS point mutations and PAX8-PPAR gamma rearrangement in thyroid tumors: evidence for distinct molecular pathways in thyroid follicular carcinoma. J Clin Endocrinol Metab 2003, 88:2318–2327
24. Davies H, Bignell G, Cox C, Stephens P, Edkins S, Clegg S, Teague J, Woffendin H, Garnett M, Bottomley W, Davis N, Dicks E, Ewing R, Floyd Y, Gray K, Hall S, Hawes R, Hughes J, Kosmidou V, Menzies A, Mould C, Parker A, Stevens C, Watt S, Hooper S, Wilson R, Jayatilake H, Gusterson B, Cooper C, Shipley J, Hargrave D, Pritchard-Jones K, Maitland N, Chenevix-Trench G, Riggins G, Bigner D, Palmieri G, Cossu A, Flanagan A, Nicholson A, Ho J, Leung S, Yuen S, Weber B, Seigler H, Darrow T, Paterson H, Marais R, Marshall C, Wooster R, Stratton M, Futreal P: Mutations of the BRAF gene in human cancer. Nature 2002, 417:949–954
25. Brose M, Volpe P, Feldman M, Kumar M, Rishi I, Gerrero R, Einhorn E, Herlyn M, Minna J, Nicholson A, Roth J, Albelda S, Davies H, Cox C, Brignell G, Stephens P, Futreal P, Wooster R, Stratton M, Weber B: BRAF and RAS mutations in human lung cancer and melanoma. Cancer Res 2002, 62:6997–7000
26. Curtin J, Fridlyand J, Kageshita T, Patel H, Busam K, Kutzner H, Cho K, Aiba S, Brocker E, LeBoit P, Pinkel D, Bastian B: Distinct sets of genetic alterations in melanoma. N Engl J Med 2005, 353:2135–2147
27. Strumberg D, Seeber S: Raf kinase inhibitors in oncology. Onkologie 2005, 28:101–107
28. Lee W, Lockhart A, Kim R, Rothenberg M: Cancer pharmacogenomics: powerful tools in cancer chemotherapy and drug development. Oncologist 2005, 10:104–111
29. Michael M, Doherty M: Tumoral drug metabolism: overview and its implications for cancer therapy. J Clin Oncol 2005, 23:205–229
30. Bond G, Hu W, Bond E, Robins H, Lutzker S, Arva N, Bargonetti J, Bartel F, Taubert H, Wuerl P, Onel K, Yip L, Hwang S, Strong L, Lozano G, Levine A: A single nucleotide polymorphism in the MDM2 promoter attenuates the p53 tumor suppressor pathway and accelerates tumor formation in humans. Cell 2004, 119:591–602

Surg Today (2006) 36:1133–1138
DOI 10.1007/s00595-006-3315-5

SURGERY TODAY

Complete Response of Highly Advanced Colon Cancer with Multiple Lymph Node Metastases to Irinotecan Combined with UFT: Report of a Case

YUJIRO FUJIE[1], MASATAKA IKEDA[1], IWAO SESHIMO[1], KOJI EZUMI[1], TAISHI HATA[1], TATSUSHI SHINGAI[1], MASAYOSHI YASUI[1], OSAMU TAKAYAMA[1], HIROKI FUKUNAGA[1], MASAKAZU IKENAGA[2], ICHIRO TAKEMASA[1], HIROFUMI YAMAMOTO[1], MASAYUKI OHUE[3], MITSUGU SEKIMOTO[1], SEIICHI HIROTA[4], and MORITO MONDEN[1]

[1]Department of Surgery, Graduate School of Medicine, Osaka University, Suita 565-0871, Japan
[2]Department of Surgery, Osaka National Hospital, Osaka 540-0006, Japan
[3]Department of Surgery, Osaka Medical Center for Cancer and Cardiovascular Diseases, Osaka 537-8511, Japan
[4]Department of Surgical Pathology, Hyogo College of Medicine, Nishinomiya 663-8501, Japan

Abstract
Massive lymph node metastasis of the para-aortic region and supraclavicular lymph nodes, Virchow's lymph node metastasis due to colon cancer, is extremely rare. We herein report a case of such systemic lymph node metastasis that was successfully treated with a combination of irinotecan (CPT-11) and UFT, a combination drug of tegafur and uracil. The patient was a 57-year-old woman who had a tumor in the ascending colon, and massively swollen para-aortic and supraclavicular lymph node metastasis. She was treated with combination chemotherapy of CPT-11 and UFT. The main tumor was detected as a decompressed scar, and the supraclavicular and para-aortic lymph nodes had completely disappeared after the second cycle of treatment. A histopathological examination and immunohistochemistry with cytokeratin showed complete remission of adenocarcinoma in the tumor and para-aortic lymph nodes. She remains alive without recurrence 52 months after chemotherapy. Combination chemotherapy of CPT-11 and UFT may be of potential value in the treatment of advanced colorectal carcinoma, and both histopathological and immunohistochemical confirmation of a complete remission may indicate prolonged disease-free survival.

Key words Colon cancer · Advanced lymph node metastasis · CPT-11/UFT · Immunohistochemistry · Complete remission

Reprint requests to: M. Ikeda, Department of Surgery and Clinical Oncology (E2), Graduate School of Medicine, Osaka University, 2-2 Yamadaoka, Suita, Osaka 565-0871, Japan
Received: September 30, 2005 / Accepted: July 25, 2006

Introduction

In colorectal cancer, 5-fluorouracil (5-FU) has been the mainstay of adjuvant treatment and treatment of metastatic disease for many years.[1] Although efforts to improve efficacy through schedule modification, including prolonged infusions, have been made, its efficacy has been limited. New agents with improved efficacy, tolerability, and ease of administration are required. Among the newer drugs, irinotecan (CPT-11) is becoming established as a first- and second-line treatment for advanced disease.[2–4] Its novel mechanisms of action have proven to be of value in 5-FU-resistant patients.

UFT is a combination drug of the prodrug tegafur and uracil in a 1:4 molar ratio.[5] Uracil is a reversible inhibitor of the enzyme dihydropyrimidine dehydrogenase (DPD), which is responsible for the catabolism of 5-FU. Combining these drugs would be anticipated to increase the response rates while maintaining the advantages of a regimen based on an orally administered fluoropyrimidine. Ohshiro et al. conducted a phase I study of CPT-11 and UFT in patients with advanced or metastatic gastrointestinal cancers, and demonstrated its safety and potential efficacy.[6] The recommended dose for a phase II study was CPT-11 150 mg/m^2 biweekly, and UFT 375 mg/m^2 on days 3–7, 10–14, 17–21, 24–28 in 4–5 weeks. They demonstrated a response rate of 42% in the 19 evaluable patients with only grade 3 adverse events of leukopenia or neutropenia.

At that time, leucovorin had not become commercially available in Japan; therefore, we conducted a phase II study of this regimen in patients with advanced or metastatic colorectal cancer to find out its safety and efficacy. We employed oral UFT-E instead of UFT capsules. UFT-E, enteric-coated granules, was designed to reduce gastrointestinal adverse events, and has been

demonstrated to have a significantly lower incidence of nausea and vomiting, while maintaining its activity.[7]

We herein report the case of a female patient with highly advanced cancer of the right colon with multiple para-aortic and supraclavicular lymph node metastases, who was recruited to this phase II study and was successfully treated with both CPT-11/UFT and surgical intervention.

Case Report

A 57-year-old woman with a 2-month history of general fatigue, abdominal discomfort, and left neck and arm swelling was referred to Osaka University Hospital. On physical examination, multiple tumors measuring up to 5 cm in diameter were palpable in the left neck and supraclavicular region. The serum carcinoembryonic antigen (CEA) level was 23 ng/ml (normal range, <5 ng/ml). All other laboratory findings were all within normal ranges.

Colonoscopy (Fig. 1A) showed type 3 advanced cancer in the ascending colon. A biopsy specimen showed poorly differentiated adenocarcinoma (Fig. 1B). A neck computed tomography (CT) scan revealed bulky swollen lymph nodes in the supraclavicular area, resulting in a complete obstruction of the left internal jugular vein and innominate vein (arrowhead, Fig. 2A). A bypassed flow around the tumors was detected as a subcutaneous contrast media (arrows in Fig. 2A). An abdominal CT scan also showed multiple lymph node swelling in the para-aortic region (Fig. 2B). Metastasis of poorly differentiated adenocarcinoma was diagnosed by fine-needle aspiration cytology of a cervical swollen lymph node. As the tumor was highly advanced, we planned to administer systemic chemotherapy. After discussing the various chemotherapeutic treatment options, the patient decided to participate in an ongoing phase II study of our institution, which is evaluating the toxicity and antitumor efficacy of combined chemotherapy of CPT-11 and UFT in patients with advanced colorectal cancer. She was fully eligible for this phase II study and written informed consent was obtained.

Treatment Schedules

According to the protocol, CPT-11 150 mg/m^2 was administered over 90 min by intravenous infusion on days 1 and 15. UFT, 375 mg/m^2 was orally administered on days 3–7, 10–14, 17–21, and 24–28. One cycle of this treatment was 35 days. The patient was treated with an actual dose of 200 mg of CPT-11 and 500 mg of daily UFT. She experienced grade 3 nausea and vomiting during the first cycle of treatment, but not during the second. She was taken off the study due to grade 4 neutropenia on day 25 of the second cycle.

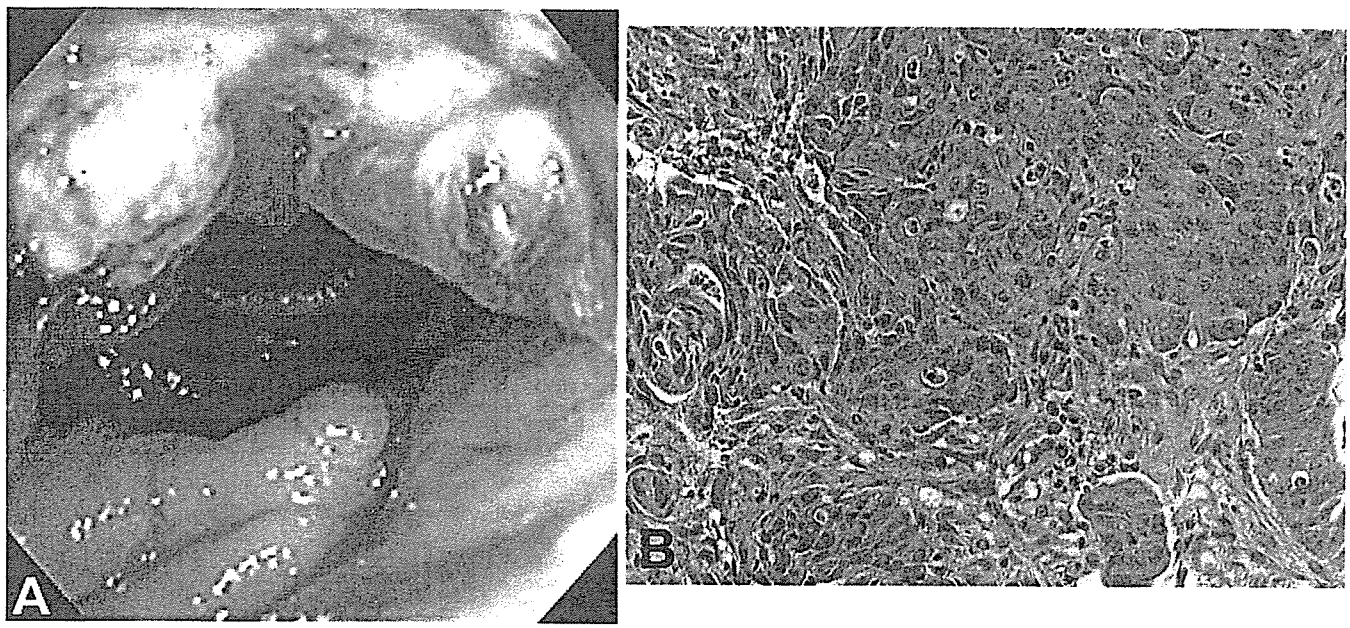

Fig. 1A,B. Colonoscopic findings at first diagnosis and a representative microscopic section of the biopsy (**B** H&E, ×200). Type 3 advanced carcinoma in the right colon. Preservation of the luminal patency and no bleeding tendency were observed. Colonic mucosa with a diffuse infiltrate of PAS-positive tumor cells and an enlarged nucleolus. Histopathological diagnosis: poorly differentiated adenocarcinoma of the right colon

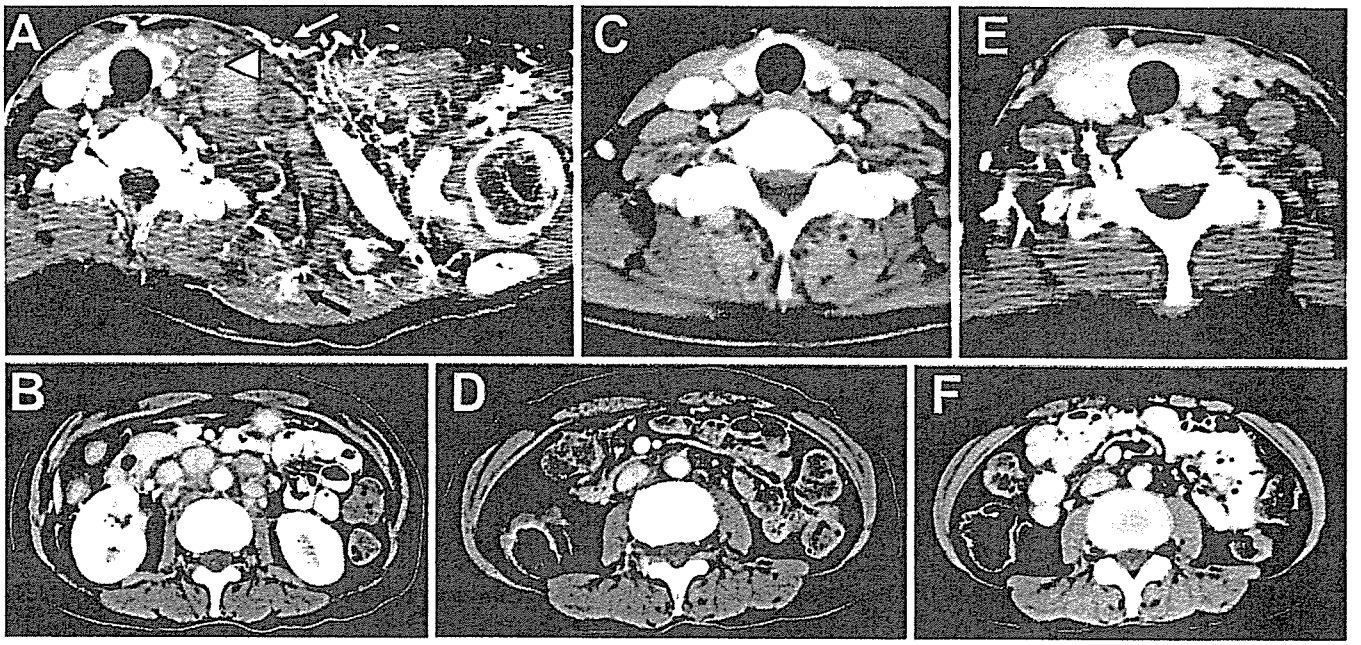

Fig. 2. Neck and abdominal computed tomography scans at first diagnosis (**A, B**), one cycle after chemotherapy (**C, D**), and two cycles after chemotherapy (**E, F**). **A** Bulky swollen lymph nodes in the left supraclavicular portion with a complete obstruction of the left internal jugular vein (*arrowhead*) and a bypassed flow around the tumors (*arrows*). **B** Multiple areas of lymph node swelling were also found in the para-aortic region. **C–F** The swollen lymph nodes at both sites decreased in size after chemotherapy

Objective Response and Toxicities

The response was evaluated by CT after each cycle, and after two cycles by endoscopy according to Response Evaluation Criteria In Solid Tumors.[8] After one treatment cycle, the supraclavicular lymph nodes had disappeared (Fig. 2C), and they still disappeared after two cycles of treatment (Fig. 2E). Para-aortic lymph nodes were also undetectable after one (Fig. 2D) and two (Fig. 2F) cycles of treatment. Figure 3A shows the endoscopic findings, i.e., that the cancer of the right colon was only a decompressed scar. Four biopsy specimens were obtained and no residual tumor was found. The serum CEA level was normalized after one cycle of treatment (3 ng/ml) and was only 1 ng/ml after the second cycle. Taken together, these parameters indicated that a complete response was obtained.

Pharmacokinetic Parameters

On day 1 of the first cycle, the fluctuation of the level of serum SN-38, an active metabolite of CPT-11, was followed before administration, and at 0, 1, 2, 8, 12, and 24 h after administration. On day 3 of the first cycle, serum levels of 5-FU before, and at 1, 2, 4, and 8 h after UFT administration were also examined. Next, the pharmacokinetic parameters, for example C_{max} (ng/ml) and AUC (ng/h/ml), were calculated. C_{max} and $AUC_{0\text{-}25.5}$ of SN-38 were 79.1 and 517, respectively. C_{max} and $AUC_{0\text{-}8}$ of 5-FU were 337 and 917, respectively.

Operation Findings

A resection of the right colon with an extended lymphadenectomy including of the para-aortic region was planned in order to remove the primary region and to make a pathological diagnosis. An upper abdominal incision was made to enter the abdomen. No evidence of ascites, liver metastasis, peritoneal dissemination, or regional lymph node swelling was detected. The primary tumor region was detected because of the scar-like serosal change; however, the tumor was not detected by palpation. A para-aortic lymph node dissection was performed at levels between the diaphragm and aortic bifurcation. Because tissues containing para-aortic lymph nodes strongly adhered to the aorta and inferior vena cava, a sharp dissection was performed to remove these tissues. End-to-side iliocolic anastomosis was done for reconstruction.

Pathological Findings

In the resected specimen, the primary region was detected only as a decompressed scar (Fig. 3B). A histopathological examination of the resected primary

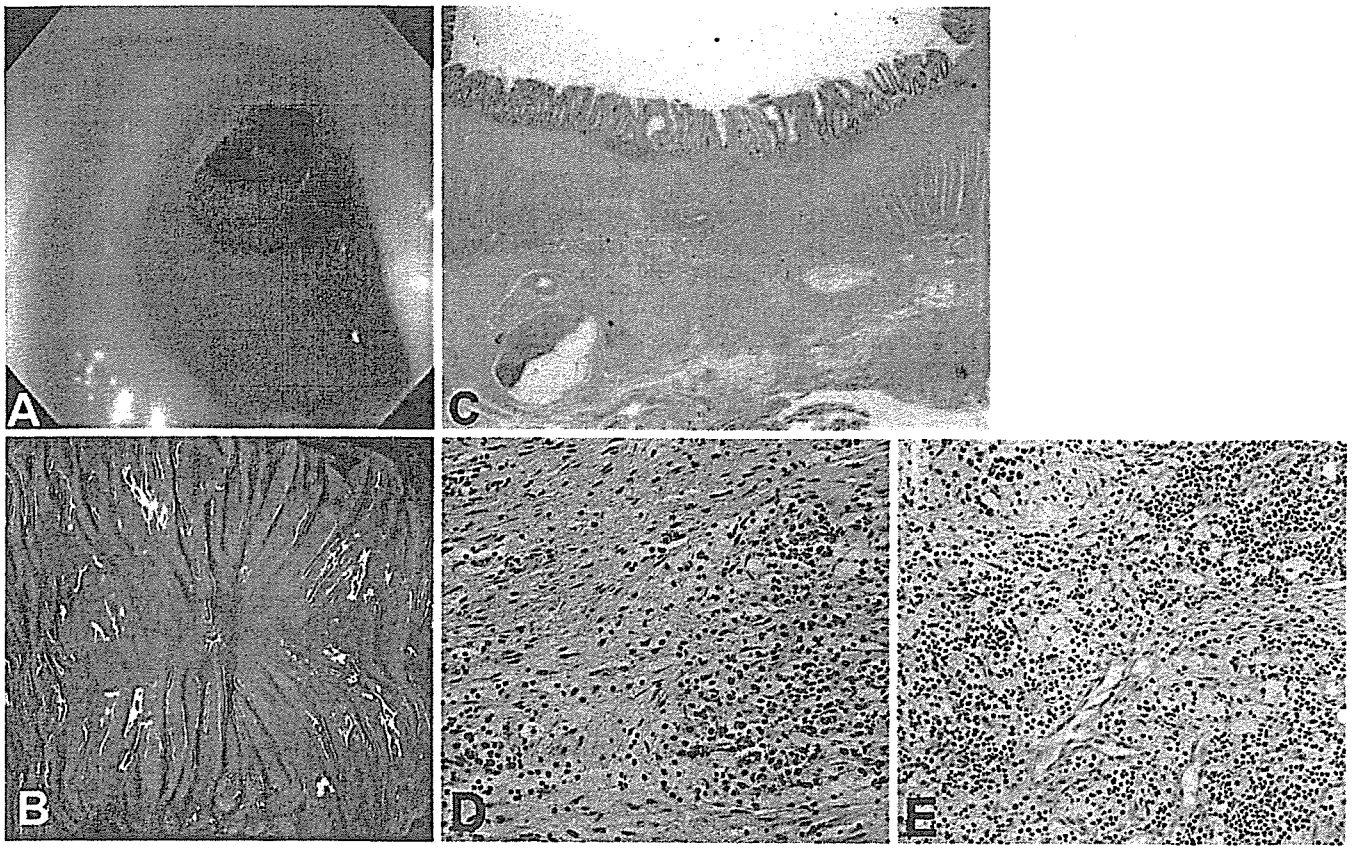

Fig. 3. A Colonoscopic findings two cycles after chemotherapy. **B** A macroscopic photograph of the resected specimen. The primary region was reduced to only a scar. **C–E** Representative sections of the resected specimen with H&E. **C** The whole appearance of the primary lesion (×12.5). The muscularis propria layer is torn, presumably by the cancer cell invasion, and this area is covered by a normal mucosa. **D,E** Strong magnification (×200) of **D** the primary lesion and **E** one of the para-aortic lymph nodes. Diffuse fibrosis and aggregation of foam cells were observed. No viable cancer cells were detected

region and para-aortic lymph nodes showed no viable cancer cells (Fig. 3C–E). Four consecutive slices of 4-μm thick sections were made from the primary tumor and all resected lymph nodes, and were subjected immunohistochemistry. Immunostaining was performed on the TechMate Horizon automated staining system (DAKO, Glostrup, Denmark), as described previously.[9] Briefly, after blocking with bovine serum albumin, the sections were incubated with pancytokeratin monoclonal antibody AE1/AE3 (DAKO, Carpinteria, CA, USA), which has been previously used for the detection of micrometastases.[10,11] This monoclonal antibody has the broadest spectrum of keratin reactivity among human epidermal keratins, and it produces positive staining in virtually all cancer cells arising from the human epithelium. They were then incubated with antimouse secondary antibody conjugated with dextran polylinker (EnVision plus; DAKO). A histological examination of biopsy specimen before chemotherapy showed positive staining with the cytokeratin antibody. However, positively stained cells were detected neither in a biopsy specimen before operation nor in the resected tumor by immunohistochemistry with cytokeratin antibody, and a histological complete remission was thus confirmed.

Postoperative Course

Because of ptosis of the stomach and paralysis of the duodenum, oral intake was insufficient for 1 month. However, it recovered thereafter and postoperative chemotherapy using CPT-11 and UFT was started 10 weeks after operation with dose modification. The patient received 150 mg/body CPT-11 and 300 mg/body/day UFT. After two cycles of treatment, she had a bowel obstruction, which required surgical intervention. After surgery she was followed up without any chemotherapy. The serum CEA level remained within the normal range and no tumor recurrence has been detected on either abdominal or neck CT. She remains alive without recurrence at 49 months after surgery.

Discussion

In colorectal carcinoma, up to 20% of all patients present with stage IV disease at initial diagnosis.[12–14] Liver, lung, and peritoneum are the most frequently observed metastatic sites. In 89 patients in the series of Scoggins et al., sites of metastasis were liver 85% (76/89), lung only 4% (4/89), and peritoneum 10% (9/89).[13] In other series of a total of 144 stage IV colorectal cancers, no case with massive lymph node metastasis was documented.[14,15] Case reports of colorectal cancer with massive lymph node metastasis including supraclavicular lymph nodes at first diagnosis are found in Japan, but the true incidence of such cases is unclear.[16–19] The prognosis of patients with stage IV colorectal carcinoma remains poor, with the median survival just 9–10.3 months,[14,20–22] and decision-making in such advanced cases is extremely difficult. Cases in which there is bowel obstruction or bleeding due to tumor progression may need a resection of the primary region.[11,12] A resection of primary and liver metastasis is recommended as long as hepatic metastasis occupies less than 50% of liver volume, although postoperative mortality and morbidity are relatively high.[13,18,20] However, decision-making in the treatment of systemic lymph node metastasis has not been fully described. Adjuvant chemotherapy following a resection of the primary tumor was performed in all case reports in Japan,[16–19] because of either bowel obstruction or no available effective regimen for neoadjuvant chemotherapy. As the prognosis of these patients was poor, another treatment strategy is necessary for patients without bowel obstruction, which requires surgical intervention. With the advent of active agents such as irinotecan and oxaliplatin,[2,3,16,23] we can anticipate different strategies for those intractable cases, i.e., down-staging by chemotherapy followed by surgical intervention. The achievement of down-staging may not only reduce operative complications but also increase the number of curatively resected cases. Because the patency of the right colon was well preserved and severe bleeding tendency was not observed under observation by colonoscopy, we thus planned to start chemotherapy on this patient.

The treatment regimen includes CPT-11 (150 mg/m^2), given as a 90-min intravenous infusion on days 1 and 15, followed by twice-daily UFT (500 mg) on days 3–7, 10–14, 17–21, and 24–28. The cycles are repeated every 35 days for two cycles. In this patient, grade 3 nonhematological toxicity (appetite loss) was noted in the first cycle and grade 4 neutropenia in the second cycle, which resulted in the cessation of UFT on day 24. C_{max} and AUC of SN-38 (CPT-11, 150 mg/m^2 administration) were previously reported as 31–42 (ng/ml) and 197–354 (ng/h/ml), respectively.[24,25] In comparison to these data, the C_{max} (79.1) and AUC (517) of SN-38 in our patient were very high. The C_{max} (337) and AUC_{0-8h} (917) of 5-FU after oral administration of UFT were also high in comparison to the findings of previous study (C_{max}: 245 ng/ml and AUC_{0-8h}: 223 ng/h/ml).[5] These results suggest that our patient was exposed to a sufficient chemotherapeutic agent, which led to a complete remission and grade 4 hematological toxicity. This patient had a bowel obstruction after two courses of postoperative chemotherapy. We still do not know the direct relationship between CPT-11 and bowel obstruction; however, CPT-11-induced colitis has been reported, which may enhance postoperative bowel adhesion.[26] We thus need to pay attention to this complication.

Continuing chemotherapy without surgical intervention might be another treatment option. Because only 2%–3% of patients have a complete response,[27] and tumor relapse after complete remission is frequently observed,[28] we carried out surgery for the purpose of histological diagnosis and cure. The confirmation of a histological complete remission with hematoxylin and eosin staining and immunohistochemistry meant that we abandoned the planned mediastinal and neck lymph node dissection. A further follow-up is definitely needed in this patient, because patients with a complete response have a long median overall survival, which is as long as 30 months.[27]

In summary, we herein reported a case of highly advanced massive lymph node metastasis from cancer of the right colon, which was successfully treated with combination chemotherapy and surgical intervention. Although a careful follow-up of this patient is obligatory, a complete pathological response was demonstrated. Combination chemotherapy of CPT-11 and UFT is thus considered to be of potential value in the treatment for advanced colorectal carcinoma.

References

1. Royce ME, Medgyesy D, Zukowski TH, Dwivedy S, Hoff PM, Pazdur R, et al. Colorectal cancer: chemotherapy treatment overview. Oncology (Huntingt) 2000;14:40–6S.
2. Cunningham D, Pyrhonen S, James RD, Punt CJ, Hickish TF, Heikkila R, et al. Randomised trial of irinotecan plus supportive care versus supportive care alone after fluorouracil failure for patients with metastatic colorectal cancer. Lancet 1998;352:1413–8.
3. Saltz LB, Cox JV, Blanke C, Rosen LS, Fehrenbacher L, Moore MJ, et al. Irinotecan plus fluorouracil and leucovorin for metastatic colorectal cancer. Irinotecan Study Group. N Engl J Med 2000;343:905–14.
4. Douillard JY, Cunningham D, Roth AD, Navarro M, James RD, Karasek P, et al. Irinotecan combined with fluorouracil compared with fluorouracil alone as first-line treatment for metastatic colorectal cancer: a multicentre randomised trial. Lancet 2000; 355:1041–7.
5. Shirao K, Hoff PM, Ohtsu A, Loehrer PJ, Hyodo I, Wadler S, et al. Comparison between the efficacy, toxicity, and pharmacokinetics of a Uracil/Tegafur (UFT) plus oral leucovorin (LV) regi-

men between Japanese and American patients with advanced colorectal cancer: Joint USA and Japan study of UFT/LV. J Clin Oncol 2004;22:3466–74.
6. Ohshiro T, Nishizaki T, Tashiro H, Matsuzaka T. Proceedings of the 39th Annual Meeting of Japan Society of Clinical Oncology, OP-1009; 2001.
7. Ohyama M, Matsumura M, Katsuta K, Nobori T, Matsuyama H, Fukami K, et al. A comparative study of UFT enteric-coated granules with UFT capsules on the occurrence of side effects in the patients with head and neck cancers. Special attention to the upper gastrointestinal tract disorders. Jpn J Cancer Chemother 1990;17:1211–6.
8. Therasse P, Arbuck SG, Eisenhauer EA, Wanders J, Kaplan RS, Rubinstein L, et al. New guidelines to evaluate the response to treatment in solid tumors. European Organization for Research and Treatment of Cancer, National Cancer Institute of the United States, National Cancer Institute of Canada. J Natl Cancer Inst 2000;92:205–16.
9. Takemasa I, Yamamoto H, Sekimoto M, Ohue M, Noura S, Miyake Y, et al. Overexpression of CDC25B phosphatase as a novel marker of poor prognosis of human colorectal carcinoma. Cancer Res 2000;60:3043–50.
10. Miyake Y, Yamamoto H, Fujiwara Y, Ohue M, Sugita Y, Tomita N, et al. Extensive micrometastases to lymph nodes as a marker for rapid recurrence of colorectal cancer: A study of lymphatic mapping. Clin Cancer Res 2001;7:1350–7.
11. Noura S, Yamamoto H, Miyake Y, Ohue M, Sugita Y, Tomita N, et al. Immunohistochemical assessment of localization and frequency of micrometastasis in lymph nodes of colorectal cancer. Clin Cancer Res 2002;8:759–67.
12. Mella J, Biffin A, Radcliffe AG, Stamatakis JD, Steele RJ. Population-based audit of colorectal cancer management in two UK health regions. Colorectal Cancer Working Group, Royal College of Surgeons of England Clinical Epidemiology and Audit Unit. Br J Surg 1997;84:1731–6.
13. Scoggins CR, Meszoely IM, Blanke CD, Beauchamp RD, Leach SD. Non-operative management of primary colorectal cancer in patients with stage IV disease. Ann Surg Oncol 1999;6:651–7.
14. Sarela AI, Guthrie JA, Seymour MT, Ride E, Guillou PJ, O'Riordain DS. Non-operative management of the primary tumour in patients with incurable stage IV colorectal cancer. Br J Surg 2001;88:1352–6.
15. Rosen SA, Buell JF, Yoshida A, Kazsuba S, Hurst R, Michelassi F, et al. Initial presentation with stage IV colorectal cancer: how aggressive should we be? Arch Surg 2000;135:530–4.
16. Baba H, Tanaka K, Kan S, Suzuki F, Otaka H, Moriya T, et al. A six-year survival case of advanced sigmoid colon cancer with metastases to both the Virchow and para-aortic lymph-nodes (in Japanese with English abstract). Nippon Shokakigeka Gakkaizasshi (Jpn J Gastroenterol Surg) 1998;31:1907–11.
17. Yamada H, Kanai M, Hamaguchi K, Ogawa H, Nakamura Y, Ohba Y, et al. Resection of colon cancer and its metastases to the Virchow lymph nodes in a patient with sarcoidosis (in Japanese with English abstract). Nippon Shokakigeka Gakkaizasshi 2002; 35:1713–6.
18. Jingu K, Nakajima Y, Inoue M, Ochiai T. A case of rectal cancer with distant lymph node metastases completely respondingto post-operative chemotherapy with levofolinate combined with 5-fluorouracil (in Japanese with English abstract). Gan to Kagakuryoho (Jpn J Cancer Chemother) 2004;31:117–9.
19. Mio H, Yamada T, Sekiya M, Maruyama H, Kathou T. A case of advanced colon cancer with metastases to both the Virchow's and the para-aortic lymph nodes that achieved complete long-term response with levofolinate/5-FU therapy (in Japanese with English abstract). Gan to Kagakuryoho (Jpn J Cancer Chemother) 2004;31:423–6.
20. Makela J, Haukipuro K, Laitinen S, Kairaluoma MI. Palliative operations for colorectal cancer. Dis Colon Rectum 1990;33:846–50.
21. Joffe J, Gordon PH. Palliative resection for colorectal carcinoma. Dis Colon Rectum 1981;24:355–60.
22. Liu SK, Church JM, Lavery IC, Fazio VW. Operation in patients with incurable colon cancer–is it worthwhile? Dis Colon Rectum 1997;40:11–4.
23. Goldberg RM, Sargent DJ, Morton RF, Fuchs CS, Ramanathan RK, Williamson SK, et al. A randomized controlled trial of fluorouracil plus leucovorin, irinotecan, and oxaliplatin combinations in patients with previously untreated metastatic colorectal cancer. J Clin Oncol 2004;22:23–30.
24. Yamada Y, Yasui H, Goto A, Arai T, Ura T, Hamaguchi T, et al. Phase I study of irinotecan and S-1 combination therapy in patients with metastatic gastric cancer. Int J Clin Oncol 2003;8:374–80.
25. Negoro S, Fukuoka M, Masuda N, Takada M, Kusunoki Y, Matsui K, et al. Phase I study of weekly intravenous infusions of CPT-11, a new derivative of camptothecin, in the treatment of advanced non-small-cell lung cancer. J Natl Cancer Inst 1991; 83:1164–8.
26. Sandmeier D, Chaubert P, Bouzourene H. Irinotecan-induced colitis. Int J Surg Pathol 2005;13:215–8.
27. Buyse MB, Thirion P, Carlson RW, Burzykowski T, Molenberghs G, Piedbois P. Relation between tumour response to first-line chemotherapy and survival in advanced colorectal cancer: a meta-analysis. Lancet 2000;356:373–8.
28. Brandi G, Pantaleo MA, Calabrese C, Di Battista M, Poggi R, Bajetta E, et al. Complete remission of primary colon cancer in a metastatic patient treated with CPT-11 plus capecitabine. Int J Colorectal Dis 2004;19:599–602.

Dig Dis Sci (2006) 51:2073–2080
DOI 10.1007/s10620-006-9410-z

ORIGINAL ARTICLE

Single-Photon Emission Computed Tomography in the Screening for Postoperative Pulmonary Embolism

Taishi Hata · Masataka Ikeda · Shoji Nakamori · Rei Suzuki · Tonsok Kim · Masayoshi Yasui · Ichiro Takemasa · Masakazu Ikenaga · Hirofumi Yamamoto · Masayuki Ohue · Takamichi Murakami · Mitsugu Sekimoto · Masato Sakon · Morito Monden

Received: 9 July 2005 / Accepted: 30 April 2006 / Published online: 15 September 2006

Abstract The aim of the study was to evaluate the usefulness of serial lung perfusion scintigraphy prospectively using single-photon emission computed tomographic image (SPECT) in screening for pulmonary embolism (PE) after elective surgery for gastrointestinal malignancy. PE was examined pre- and postoperatively with SPECT. Diagnosis of PE was based on segmental perfusion defect visualization in at least two of three planes on a SPECT image compared with preoperative SPECT images. Final diagnosis was determined by detection of embolus with multidetector helical CT (MDCT). No perioperative anticoagulant was used. Thirty-four patients were enrolled. One patient was excluded because of thrombophilia. In preoperative scans, nonsegmental defects were detected in 11 and a segmental defect in 1 patient, who was then diagnosed as PE preoperatively. Among 21 patients with normal preoperative SPECT, 2 had nonsegmental and 5 had segmental defects postoperatively. Among 11 patients with nonsegmental preoperative SPECT, 7 had nonsegmental and 4 had segmental defects postoperatively. Postoperative segmental defects were differentiated by their shape only and there was no need to compare pre- and postoperative SPECT. MDCT confirmed four patients with PE among nine with segmental defects postoperatively. Our results of screening for PE by visualization at least two planes of SPECT images suggest that postoperative SPECT scan is suitable for the diagnosis of postoperative PE.

Keywords Pulmonary embolism · Single-photon emission computed tomographic image (SPECT) · D-dimer · Gastrointestinal cancer

T. Hata · M. Ikeda (✉) · R. Suzuki · M. Yasui · I. Takemasa · H. Yamamoto · M. Sekimoto · M. Monden
Department of Surgery, Department of Surgery (E2), Graduate School of Medicine, Osaka University,
2–2 Yamadaoka, Suita, Osaka 565-0871, Japan
e-mail: mikeda@surg2.med.osaka-u.ac.jp

S. Nakamori · M. Ikenaga
Department of Surgery, Osaka National Hospital,
Osaka, Japan

T. Kim · T. Murakami
Department of Radiology, Graduate School of Medicine,
Osaka University,
Osaka, Japan

M. Ohue
Department of Surgery, Osaka Medical Center for Cancer and Cardiovascular Diseases,
Osaka, Japan

M. Sakon
Department of Surgery, Nishinomiya Municipal Hospital,
Hyogo, Japan

Introduction

Pulmonary embolism (PE) is a major postoperative complication after surgery for malignancy [1, 2]. The incidence of clinically symptomatic PE without prophylaxis after surgery for gastrointestinal malignancy is estimated at about 4.0% to 10.0% according to the Guideline of Sixth American College of Chest Physicians Consensus [3]. It is therefore essential to establish early and accurate diagnosis in patients with suspected PE. However, the diagnosis of PE is sometimes difficult because the clinical symptoms are nonspecific and limitations of the available objective tests. Lung ventilation/perfusion (V/Q) scan is recommended by the American Thoracic Society [4] and the European Society of

Cardiology [5] as the first-line examination, if there is a clinical suspicion of PE. Lung V/Q scan is sensitive, but was long believed not to be specific enough to establish the diagnosis of PE. This opinion was based on the correlative findings with pulmonary angiography, which was once regarded as the gold standard in the detection of PE. Today no gold standard in the diagnosis of PE is clinically available [6] and the sensitivity of pulmonary angiography is obviously at the magnitude of only 70% [7], which is too low for clinical use. The Prospective Investigation of Pulmonary Embolism Diagnosis (PIOPED) criteria, obtained by comparison with pulmonary angiography [8], have been used for the diagnostic reading of V/Q scans. However, by these criteria [9, 10], only high-probability and normal or very low-probability scans are diagnostic, and considerable numbers of patients (73%) fall within nondiagnostic categories that are intermediate- and low-probability scans. Combining well-characterized clinical estimates of PE with independent interpretation of perfusion lung scan alone, the Prospective Investigative Study of Acute Pulmonary Embolism Diagnosis (PISA-PED) study group could limit patients who require further angiographic evaluation [11]. They concluded that accurate diagnosis of PE is possible by perfusion scanning alone, without ventilation imaging. However, by doing this, the sensitivity of perfusion scanning is artificially reduced in order to approach that of pulmonary angiography. Nonsegmental perfusion defects representing PE may be missed by this, and this problem may be overcome by comparison of pre- and postoperative scans.

In recent years, perfusion lung scan with the single-photon emission computed tomographic (SPECT) technique has been introduced, and its usefulness over the conventional planar perfusion scan has been demonstrated [12, 13]. SPECT has a higher spatial resolution so it can detect abnormalities, particularly on the subsegmental level [12] and in the lung bases, where the segments are tightly packed [14]. On the other hand, it may also detect preexisting pulmonary abnormalities because of its good spatial distribution, which could weaken the usefulness of SPECT. Palla et al. [15] reported lung SPECT had high sensitivity, but had low specificity, because it detects defects that have no angiographic correlates when at least one plane segmental defect was considered PE. Since several studies have demonstrated the usefulness of serial planar scintigraphy for the screening of postoperative PE by direct comparison of pre- and postoperative images [16, 17], we hypothesized that postoperative PE could be diagnosed more precisely with the use of SPECT pre- and postoperatively.

In this study, we prospectively investigated the usefulness of serial examination of lung SPECT for the detection of PE after elective gastrointestinal malignancy surgery.

Patients and methods

Study design

This was a prospective study involving patients who were elected to undergo surgery for sigmoid colon cancer, rectal cancer, or pancreatic cancer. Patients were eligible for the study if they were 20 years or older, had normal laboratory findings for thrombophilia, and gave written informed consent. Patients were excluded if they had accompanying disease, such as acute myocardial infarction, chronic obstructive pulmonary disease, and stoke, and had a history of venous thromboembolism and anticoagulant therapy. Another reason for noninclusion was the attending doctor's decision on unsuitability for the study. The study was approved by the Ethics Committee of Osaka University. Recruitment of patients began in August 2001 and ended in December 2002. Patients underwent preoperative evaluation of PE with lung perfusion SPECT (baseline data) and chest x-ray (baseline data). Arterial blood gases and laboratory tests (complete blood count, D-dimer, and thrombin-antithrombin complexes [TAT]) were also performed preoperatively. Thrombosis prophylaxis was performed with both mechanical pneumatic compression and graduated compression stockings for lower extremities until patients were ambulatory, but no perioperative anticoagulants were administered. Signs and symptoms of deep venous thrombosis (DVT) and PE were recorded postoperatively. Chest x-ray, arterial blood gas, and laboratory tests were also serially performed postoperatively and lung perfusion SPECT was carried out 7–9 days after the operation. Figure 1 shows a flowchart of the study protocol.

Diagnostic methods

All perfusion lung SPECT studies were performed with an LEHR parallel-hole collimator (GCA-9300 A/HG; Toshiba). The isotope modeled was ^{99m}Tc-macroaggregated albumin (MAA), 185 MBq, administered intravenously with the patients in the supine position. All images were acquired with a triple-detector scintillation camera. A 360° SPECT acquisition of the ventilation scan was performed using a 128 × 128 matrix. A 120° rotation per head was done in 20 steps of 20 sec each (total acquisition time, 400 sec). Images were reconstructed by filtered back-projection using a Butterworth filter (cutoff frequency, 0.2; order, 8). No attenuation correction was applied. The effective dose for SPECT is 2.2 mSv. Images were formatted 9.6 mm thick for transverse, coronal, and sagittal views. Each preoperative and postoperative SPECT study was interpreted by at least two doctors at the time of completion of the scanning. Every perfusion defect was classified as segmental or nonsegmental according to its appearance in pre- and postoperative SPECT images.

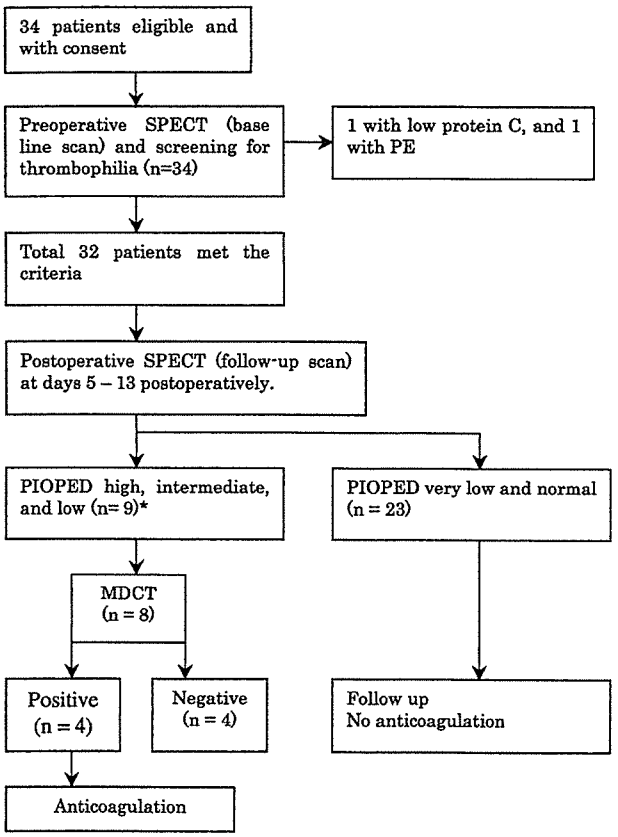

Fig. 1 Flowchart of the study protocol. *Postoperative SPECT was evaluated according to the PIOPED criteria in comparison with baseline scan

The segmental appearance was defined as a wedge-shaped morphology, with the sharp angle oriented toward the corresponding segmental artery. A nonanatomical defect, which did not correspond to a specific segment, was defined as nonsegmental. Because the diagnostic criteria of SPECT for PE have never been properly validated, we followed the criteria used by Touya et al. [18], i.e., segmental visualization in at least two of three planes on a SPECT imaging was considered to be evidence of PE. Defect areas were classified according to the size of defects, i.e., small defects (<25% of a segment), moderate defects (25%–75% of a segment), and large defects (>75% of a segment). When defect numbers and areas of postoperative SPECT were ≥ 4 small defects, ≥ 1 segmental small defects, 1 moderate to <2 large defects, 1 large defect and ≥ 2 moderate defects, or ≥ 2 large defects, four-slice multidetector helical computed tomography (MDCT) with contrast medium (2.5 mm thick) was carried out. MDCT was performed within 48 hr of SPECT evaluation and analyzed during the course of clinical workup by one experienced radiologist and two surgeons. The usefulness of serial SPECT was assessed by comparison of baseline image and postoperative image.

CT images were obtained with a helical scanner (GE Medical Systems, Milwaukee, WI). A total of 50 ml of the nonionic contrast agent iopromide containing 300 mg iodine per milliliter was administered with a power injector at an injection rate of 5.0 ml/sec. Helical CT scanning was performed with 2.5-mm collimation, 7.5-mm table increment per gantry ratation (HQ mode), a tube voltage of 120 kV, and a tube current of 200 mA, and was started 6 sec after initiation of injection of the contrast material to achieve adequate enhancemet in the pulmonary arteries during the course of scanning. With the condition of 20-cm scan for coverage of the pulmonary artery, the weighted CT dose index (CTDIw) and volume CT dose index (CTDIVolume) were 16.2 and 21.6 mGy, respectively. The effective dose was 8.6 mSv. Transaxial images were reconstructed at 1.25-mm increments (2.5-mm slice thickness) on a 512 × 512 matrix. A window width of 350 HV and center of 35 HV were chosen for all images.

Statistical analysis

Data were processed and analyzed by StatView 5.0 (SAS institute Inc., Cary, NC). Statistical analysis was performed with unpaired *t*-test. P values of < 0.05 were considered statistically significant.

Results

Baseline SPECT

The study subjects were 34 patients and included 8 patients with pancreatic cancer, 18 with rectal cancer, 7 with sigmoid colon cancer, and 1 patient with transverse colon cancer who had been diagnosed preoperatively as sigmoid colon cancer. Laboratory tests showed a low level of protein C (52%) in one patient, who was subsequently excluded from the study (Fig. 1). Baseline SPECT scan showed 16 defects in 12 patients (36%) (Table 1). One patient had two nonsegmental defects and one segmental defect (Fig. 2 and Table 1). As two planes of this defect showed a large segmental defect, this patient was suspected for PE, and MDCT was performed. Although MDCT failed to show an embolus in the pulmonary artery, thrombus in the left popliteal vein was detected. He

Table 1 Number of defects detected in pre- and postoperative lung SPECT

Defects	Preoperative scan ($n=33$)	Postoperative scan ($n=32$)
Nonsegmental	13 (2)[a]	19 [11][b]
Segmental	0 (1)	14 [0]
Total	13 (3)	33

[a]Number of defects detected in patients with preoperative pulmonary embolism in parentheses.

[b]Number of defects detected in the preoperative scan in brackets.

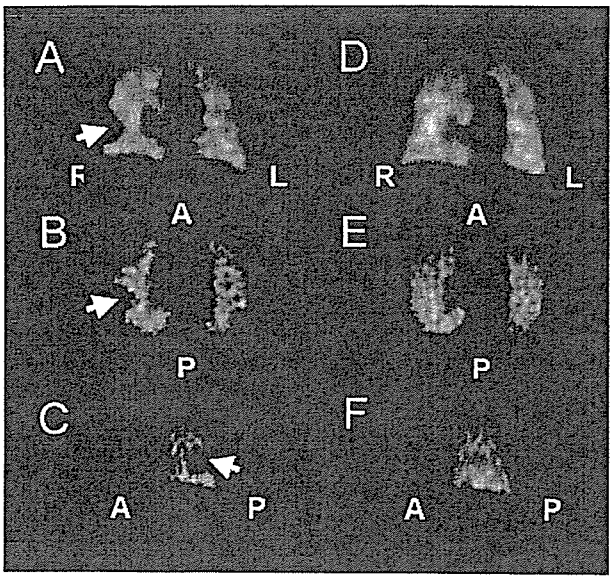

Fig. 2 Baseline SPECT (A–C) and posttreatment SPECT (D–F) in a patient with preoperative pulmonary embolism. Defects are marked by arrows. SPECT, single-photon emission computed tomography; R, right; L, left; A, anterior; P, posterior

was excluded from the study and anticoagulant therapy was initiated. No abnormal defect was found on SPECT after 2 weeks of anticoagulation (Fig. 2). The detailed clinical course of this patient was reported [19]. The other 13 defects in 11 patients were all nonsegmental (Table 1); 2 patients had two nonsegmental defects and the other 9 patients had one nonsegmental defect. There was no abnormal finding in preoperative chest x-ray in relation to these 13 nonsegmental defects.

During preoperative evaluation, 2 patients were excluded from the study, resulting in 32 patients who met the selection criteria (Fig. 1). Table 2 reports the details of the clinical characteristics of the 32 patients.

Postoperative SPECT

A total of 32 patients underwent postoperative SPECT. We performed SPECT on postoperative day 2 in one patient because of dyspnea, which was highly suspicious for PE. For the other patients, SPECT was performed between postoperative days 5 and 13 (median, day 6). We found 33 defects in 18 patients in postoperative SPECT images; 19 defects were nonsegmental and 14 defects were segmental (Table 3). Nine patients had nonsegmental defects only (total number of defects, 11), and nine patients had segmental defects. Five of the nine patients with segmental defects also had nonsegmental defects (total number of defects, eight). None of the segmental defects was due to lung parenchymal changes such as bulla, pleural effusion, and atelectasis as confirmed by CT or chest x-ray. Two of nine patients with two or more large defects had clinical symptoms of dyspnea

Table 2 Patient characteristics

Mean age (SD), yr	60 (9.4)
Male:female	19:13
Disease	
Transverse colon cancer	1
Sigmoid colon cancer	7
Rectal cancer	18
Pancreatic cancer	6
Operative procedure	
Sigmoidectomy	5
Anterior resection	1
Low anterior resection	13
Abdominoperineal resection	3
Total pelvic exoneration	3
Transverse coloctomy	1
Distal pancreatectomy	3
Pancreaticoduodenectomy	2
Exploratory laparotomy	1
Operation time (min), mean (SD)	350 (221)
Blood loss (g), mean (SD)	1231 (1563)

or chest pain and underwent MDCT, which detected an embolus in the pulmonary artery in each case. One of these two patients was also found to have DVT in the popliteal vein. Six of the other seven patients underwent MDCT in search of emboli, and an embolus was detected in the pulmonary artery in each of two patients, one of whom had a thrombus in the soleus vein. One patient had a thrombus in the femoral vein only, and no thrombus was detected in the pulmonary artery.

Anticoagulant therapy consisting of intravenous heparin followed by warfarin was initiated in all five patients with PE or DVT. The other four patients were followed up conservatively without any anticoagulant therapy and showed an uneventful recovery. Exemplary cases of patients with confirmed PE are shown in Fig. 3 and those with only segmental defects are shown in Fig. 4. A new segmental defect not present on the baseline scan was detected in each of the five patients, but a definite diagnosis of PE was not made by MDCT. These were not attributable to infiltrate, pleural effusion, or atelectasis in vascular congestion on the chest x-ray and MDCT and were strongly suggestive of PE.

Comparison of baseline and postoperative SPECT

Comparison of baseline and postoperative images showed that 11 of 13 nonsegmental defects detected preoperatively were also detected as nonsegmental defects in the postoperative SPECT (Table 1). The other two defects were not detected postoperatively. In contrast, 11 of 19 postoperative nonsegmental defects had been detected on the baseline images, and the other 8 were new. All 14 segmental defects were newly detected on postoperative SPECT (Table 1).